Review Article *Open Access*

Journal of Modern Classical Physics & Quantum Neuroscience

ISSN: 3068-4196

DOI: *doi.org/10.63721/25JPQN0109*

Plasma Control in a Tokamak-Type Machine Using only Magnetic Measurements

Bernard Bareyt

Independent Researcher, Belgium

Citation: Bernard Bareyt (2025) Plasma Control in a Tokamak-Type Machine Using Only Magnetic Measurements. J.of Mod Phy & Quant Neuroscience 1(3), 01-55. WMJ/JPQN-109

Abstract

The "clean" nuclear energy of tomorrow will probably be produced using Tokamak-type machines, despite the technological difficulties. Thermonuclear fusion based on the Tokamak process is more promising than that based on other types of fusion machines such as the "Stellarator" process or even inertial fusion, a field reserved for the military. For cost-effective energy production, with the Tokamak process, and discharge times of several tens of minutes, followed by downtime, the machine's windings must be made using superconductors. Finally, plasma control must be simple, reliable and efficient in order to optimize energy exchanges between the plasma and the outside world. For this reason, we propose in this paper to show that the control of the plasma equilibrium and that of the plasma current amplitude are quite feasible, in a simple and efficient way using only magnetic measurements installed inside the vacuum chamber, mainly absolute flux measurements. For machines with or without iron core or with or without magnetic « divertor », the flux deviations, calculated on the presumed plasma contour, are then fed back to the voltages of the poloidal field coils alone through a high-performance control loop. Based on this approach, neither coupling with numerical simulation data nor any knowledge of the plasma profile is necessary in real time. We will show that there is a particular closure matrix of the plasma position control loop that allows high loop gains, decoupled from the vacuum chamber and independent on the presence of a magnetic core. Finally, for machines with "divertor", the control of the plasma and that of the zero field points become practically independent thanks to a pre-programming voltage applied to the poloidal field coils, thus promoting control of free zero field points.

***Corresponding author:** Bernard Bareyt, Independent Researcher, Belgium.

Submitted: 05.06.2025 **Accepted:** 11.06.2025 **Published:** 18.08.2025

Keywords: Nuclear Magnetic Resonance (NMR), Spin- Spin Interaction, Energy States in NMR, Coupling Constants in NMR, Clebsch-Gordan Coefficients

1. Scope of application

In this document, we propose to present and then address all the problems related to the control of plasma movements and the amplitude of the plasma current, in a "Tokamak" type machine whose geometry is toroidal; that is to say that the contours of the plasma, the vacuum chamber and the external coils are generated by a vertical section: 2D, rotating around a vertical axis as shown in the following Figure 1.

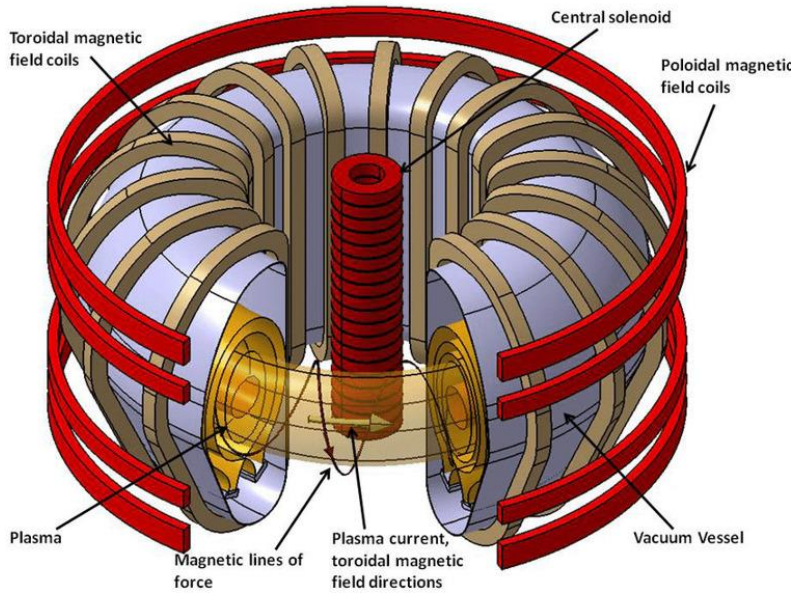

Figure 1: Diagram of a Tokamak

Given the toroidal geometry, all formulations of magnetic fields and fluxes can be defined in a cylindrical coordinate system: r, θ, z, i.e. the polar coordinates in the horizontal plane (r, θ) to which we add the height of the point relative to the horizontal plane: z, and which are expressed in Cartesian coordinates by:

$$x = r * \cos(\theta)\,;\;\; y = r * \sin(\theta)\,;\;\; z$$

The general case of machines in the air, therefore without a magnetic circuit, will first be fully treated up to § 7, inclusive. The influence of the magnetic circuit will then be detailed in § 8. Finally, the presence of a single or double magnetic "divertor" will be treated in § 9.

1.1. Aim

This document aims to analyze, understand and translate the behaviour of the plasma seen by an external observer and then to deduce the laws linking the plasma movements to the magnetic measurements in a Tokamak. Finally, this study will determine the method(s) for controlling the plasma in a Tokamak with or without a magnetic core and with or without a magnetic "divertor".

We will show that plasma control can be simply achieved using magnetic measurements alone. Plasma physics associated with numerical simulations would only be used to demonstrate its physical feasibility. The main law: "Plasma contour iso flux", is true whatever is the plasma current profile.

Finally, this project requires the development of easy-to-use tools for calculating the different magnetic configurations and optimizing the plasma control loop.

1.2. Definitions and hypotheses

We will assume up to § 7, inclusive that the machine has neither magnetic core nor magnetic divertor. The equations linking the fluxes and currents by mutual inductances are calculated in air or vacuum (relative magnetic permeability: μr = 1), therefore linear.

The different contours carrying or likely to carry a current distribution are:

- The external poloidal field coils, located around the vacuum chamber (index: b, for all the coils on the contour: Cb).
- The vacuum chamber containing the plasma (index: c of the contour),
- The plasma whose external contour bears the index: p (or 1),
- The windings associated with the magnetic divertor bearing the index: d.

The modelling of a discrete conductor such as a thick coil, the vacuum chamber or the plasma contour will be carried out by a set of coaxial circular conductors of large radius R and small radius r, located in the conductor section.

Finally, all the current distributions will be defined in ampere-turns: J. This definition affects the poloidal field coils and those of the magnetic "divertor", consisting of multi-turn windings: N, traversed by a current: I, such that: $J = N * I$. It follows that the electrical voltages of the coils and the associated power generators will also be defined for 1 turn, i.e.:

$$v = \frac{V}{N}$$

1.3. General remarks

Finally, almost all the problems treated in this document call upon the classical laws of electromagnetism, accessible to all, including the calculations of magnetic fields and fluxes. Only some problems call upon linear optimization methods with constraints whose explanations and methods are, I think, simple and understandable.

Furthermore, all the calculations listed in this document were carried out with "Microsoft Excel", accessible to all. My wish is to make accessible and exploit the laws that have remained "mysterious" for too long regarding the movements of plasma in a Tokamak and from this to deduce simple methods for controlling the plasma displacements and the plasma current.

All the steps of this project require, for the reader, simple and understandable demonstrations, even if some have already been published in the past in one or more scientific journals. This document therefore has the advantage of bringing together all the knowledge and know-how necessary to resolve the problems associated with controlling plasma in a Tokamak based solely on magnetic measurements.

2. Foreplay

Before addressing the real problems of plasma control, it seems necessary to introduce the notion of virtual hull or shell and its properties which will help us to understand and translate the electromagnetic phenomena encountered in a Tokamak.

2.1. Definition of the virtual shell

The virtual shell is defined as a mechanically robust, flexible, and freely deformable closed contour: Cv, with an ultra-thin shell thickness. Finally, the shell is superconducting, its main property; that is to say that its electrical resistance is zero, therefore generating no loss by joule effect.

2.2. General properties of the virtual hull or shell

2.2.1. Virtual shell electromagnetic equation

Consider a virtual shell placed on a closed contour Cv. Let: $\emptyset v$, the distribution of the magnetic flux on the contour Cv and Jv, the distribution of current located on the shell merged on the contour Cv.

The behaviour of the virtual shell is translated by the equation:

$$\emptyset v = 0,$$

on all points of the contour Cv, where: $\emptyset v$ is the flux of the virtual shell. In other words, if: $d\emptyset v_{ext}$, represents the external flux variation generated on the contour Cv, including the deformations of the contour or its relative displacements with respect to the other conductors, then the shell reacts by a current variation: dJv, induced such that:

$$d\emptyset v_{ext} + MVV * dJv = 0,$$

With: MVV, the matrix of mutual inductances between conductors modelling the shell.

2.2.2. Moving and deforming the virtual hull in a magnetic field

Any external flux variations applied to the contour of the virtual shell, due to displacements, deformations of the shell, as well as relative displacements of the shell in relation to the external conductors, result in:

$$d\emptyset v_{ext} = dMVV * Jv + \sum dMVX * Jx, \text{ with x, the index of the external or internal conductor to Cv}$$

which instantly changes the current distribution dJv such that:

$$MVV * dJv + d\emptyset v_{ext} = 0$$

where: MVV is the matrix of mutual inductances between conductors modeling the shell.

2.2.3. Electromagnetic energy of a virtual shell and consequences

The electromagnetic energy of the virtual shell is always identically zero, because whatever the induced current distribution: Jv, the flux on the contour Cv is identically zero: $\emptyset v = 0$.

This means that the shell cannot modify the existing magnetic configurations, internal and external, in which it is placed.

In other words, the displacement or deformation of the virtual shell in a magnetic field does not generate any induced current in the conductors external or internal to the shell.

2.2.4. Partitioning of internal and external magnetic configurations

The virtual shell establishes an electromagnetic partition between the interior and exterior spaces at Cv where the internal and external magnetic configurations evolve independently, therefore without mutual interference.

Consider a set of conductors located inside and outside the virtual shell Cv then, any variation of the flux on Cv: $d\emptyset v_{ext}$, due to the external magnetic configuration, immediately leads to the appearance of an induced current: dJv, on the surface of the shell which opposes the penetration of the flux inside Cv. The conductors inside the shell therefore do not "see" any variation of flux on Cv, because: $\emptyset v = 0$; therefore, the internal magnetic configuration is not altered by the electromagnetic variations external to Cv.

Similarly, any modification of the internal magnetic configuration does not alter the external magnetic configuration.

2.2.5. Placing a virtual shell on a closed contour

The value of the initial current distribution: Jv_o, induced on the virtual shell, when placed on a fixed contour Cv, depends only on the flux distribution: $\emptyset v_{ext}$, on the contour Cv, existing before the placement of the shell, according to the equation:

$$MVV * Jv_o + \emptyset v_{ext} = 0.$$

2.2.6. Virtual shell and reality

The equation: $\emptyset v = 0$, with a virtual shell, means that any variation of the flux applied to the virtual shell due to the changes of the external and/or internal magnetic configurations results in an induced current distribution on the shell.

In reality, therefore without a virtual shell, the equation: $\emptyset v = 0$, simply translates that the Cv contour is a zero-iso flux contour.

3. Principles of the virtual hull applied to a Tokamak

3.1. Definition and properties of magnetizing current distribution

3.1.1. External magnetizing current distribution

Consider a space located in vacuum or air where the magnetic flux: $\emptyset o$, is constant throughout the space and a closed contour Cv located in this space. Let us imagine that we place a virtual shell on this contour Cv, then a current distribution: Jv, is instantly induced on the shell, according to the law: $\emptyset v = 0$, opposing the passage of the constant flux inside the virtual shell where the fields and fluxes are identically zero, according to Figure 2.

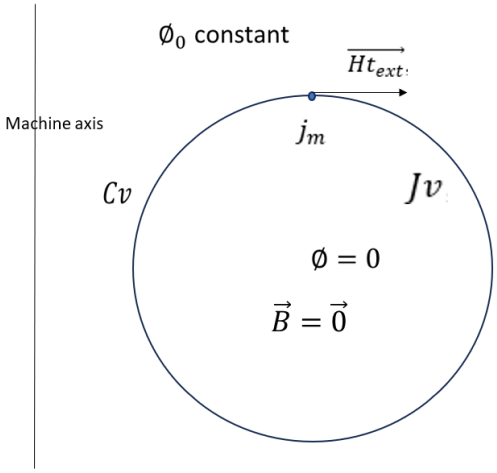

Figure 2: Virtual shell inserted in a constant flux space

In reality, as there is no virtual shell, the current distribution: Jv, simply cancels the fluxes on Cv, thus maintaining the contour Cv zero-iso flux. This particular distribution: Jv, generates, alone on the contour Cv, a constant flux: $-\emptyset o$, opposite to the external flux. The internal magnetic configuration at Cv being identically zero, there therefore only remains the external tangent field: $\overrightarrow{Ht_{ext}}$, at the contour Cv. The evaluation of: $\overrightarrow{Rot}(\vec{H})$, on the contour Cv, expresses the relation linking the external tangent field to the local linear current density of Jv on Cv:

$Ht_{ext} = \rho_m$, with: ρ_m = linear current density of the magnetizing current distribution Jv on Cv.

This particular current distribution, called: the "external magnetizing distribution" at the Cv contour, generates a constant flux on the Cv contour and a distribution of null magnetic field, inside Cv. It follows that any contour located inside an iso flux contour is also iso flux. For this reason, the external magnetizing current distribution will always be evaluated on the same contour as that of the flux evaluation, i.e.:

Equation 1: External magnetizing current distribution on the closed contour: Cv

$MVV * Jv_m = \emptyset v_m$; Cv iso flux and $\vec{H} = \vec{0}$, inside Cv.

3.1.2. Internal magnetizing current distribution

The internal magnetizing current distribution at the contour Cv is defined by the current distribution: Ji_m, located on a contour: Ci, inside Cv, which maintains the contour Cv iso flux.

Equation 2: Internal magnetizing current distribution on the closed contour Cv

$MVI * Ji_m = \emptyset v_m$, iso flux on the contour Cv and Ci interior to Cv.

3.2. Interior Cv contour to an exterior current distribution

Consider a closed contour: Ce, carrying an external current distribution: J_{ext}, and a closed contour: Cv, located inside Ce, according to Figure 3. The distribution: J_{ext}, creates on the internal contour Cv, an initial distribution of tangential fields: $\overrightarrow{Ht_o}$, on Cv.

Now imagine that we place a virtual shell on the internal contour Cv. Then, a current distribution: Jv, is instantly induced on the shell according to the law: $\emptyset v = 0$.

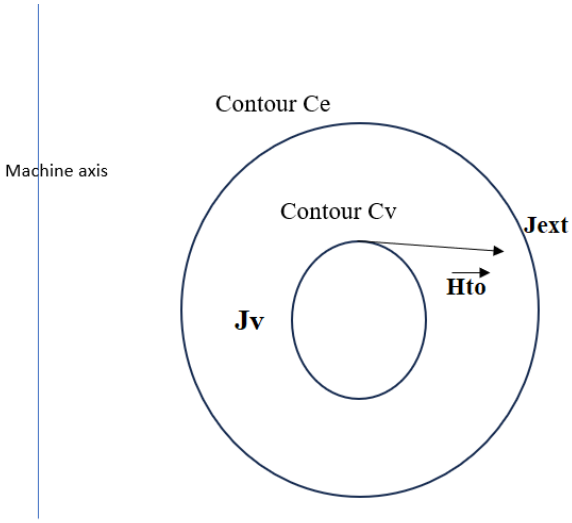

Figure 3: Virtual shell surrounded by external conductors

Since $\emptyset v = 0$ and there is no current distribution inside Cv, we deduce that the fluxes and fields are null inside Cv. Thus, the internal fields tangential and normal to the contour Cv are zero:

$$Ht_{int}=0 \text{ and } Hn_{int}=0$$

It follows that the external normal field being equal to the internal normal field is also zero (continuity of the normal field):

$$Hn_{ext}=0$$

Only the non-zero external tangential field remains: Ht_{ext}, created by the distribution: Jv, which has a magnetizing component. The evaluation of: $\overrightarrow{Rot}(\vec{H})$, on the contour Cv is translated, after decomposition of the distribution: Jv, according to the external magnetizing component and the component with zero-ampere-turns, by:

Equation 3: Relationship between the external tangent field at Cv and the current density of Jv

$$Ht_{ext} = H_e + H_m = \rho_e + \rho_m \rightarrow H_e = \rho_e \text{ and } H_m = \rho_m$$

- $\rho_e =$ linear density of the zero-ampere-turns component of Jv,
- $\rho_m =$ linear density of the magnetizing component of Jv, generating a uniform flux on Cv and a zero-field inside Cv.
- H_e and H_m, are the components of the external field specific to current densities: ρ_e and ρ_m.

In reality, since there is no virtual shell, the current distribution: Jv, cancels the fluxes on Cv and the fluxes and fields inside Cv, thus maintaining the contour Cv at zero iso flux, in the presence of the external current distribution: J_{ext}. As a corollary, the current distribution: $-Jv$, alone on the contour Cv, generates the magnetic configuration initially created by the distribution: J_{ext}, inside Cv.

The magnetizing component of: $-Jv$, alone on Cv, and of linear density: $-\rho_m$, generates a uniform flux and a zero-field inside Cv.

The zero-ampere-turns component of the distribution: $-Jv$, alone on Cv and of linear density: $-\rho_e$, generates the magnetic field inside Cv.

The distribution: $-Jv$, being an external distribution with respect to the internal magnetic configuration of Cv, the tangent fields at Cv are therefore the interior tangent fields inside Cv, whose component, on Cv, is necessarily equal to the initial field: $\overrightarrow{Ht_o}$. By calculating the rotational of the magnetic field on Cv, we obtain the relationship between the initial tangent fields and the linear current density: ρ_e, of the null ampere-turns distribution of Jv:

Equation 4: Relationship between the initial tangent field at Cv and the current density ρ_e of Jv

$$\rho_e = Ht_0 = H_e$$

3.3. Cv contour encircling an interior current distribution

Consider an inner closed contour: Cp, carrying a current distribution: Jp, and a closed contour: Cv, located outside Cp, according to Figure 4. The inner current distribution: Jp, creates on the outer contour Cv, an initial distribution of tangential fields: $\overrightarrow{Ht_o}$.

Now imagine that we place a virtual shell on the outer contour Cv. Then, an initial current distribution: Jv, is induced instantaneously on the shell according to the law: $\emptyset v = 0$.

This current distribution: Jv, cancels the fluxes on Cv and the fluxes and fields outside Cv. Since there is no current distribution outside Cv, we deduce that the external fields tangential and normal to the contour Cv are zero:

$$Ht_{ext} = 0 \text{ and } Hn_{ext} = 0$$

It follows that the internal normal field being equal to the external normal field is also zero (continuity of the normal field):

$$Hn_{int} = 0$$

Only the non-zero internal tangential field remains: Ht_{int}. The evaluation of: $\overrightarrow{Rot}(\vec{H})$, on the contour Cv results in:

Equation 5: Relationship between the internal tangent field at Cv and the current density of Jv

$Ht_{int} = -\rho_v$, with: ρ_v= linear current density of Jv on Cv

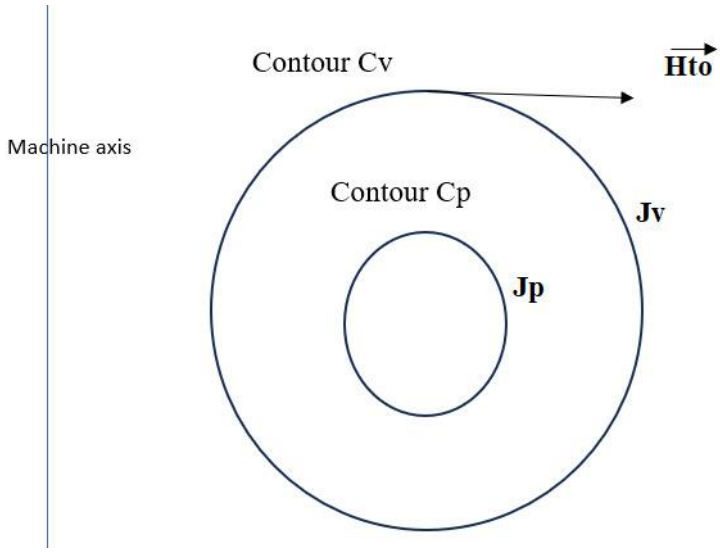

Figure 4: Virtual shell surrounding inner conductors

In reality, since there is no virtual shell, the current distribution: Jv, cancels the fluxes on Cv and maintains the contour Cv at zero-iso flux. In addition, the fluxes and the fields outside Cv, whose initial external tangent fields, are cancelled by the distribution: Jv.

In conclusion, as the current distribution: Jv, cancels the flux on Cv and the fields and fluxes outside Cv, the opposite distribution: $-Jv$, alone on Cv, generates the magnetic configuration outside to Cv, initially created by the internal distribution: Jp, whose distribution of the initial external tangent fields: Ht_0, on Cv. We deduce by calculating: $\overrightarrow{Rot}(\vec{H})$, on Cv that:

Equation 6: Relationship between the initial field Ht_0 and the distribution Jv

$Ht_0 = -\rho_v$, i.e. from Equation 5: $Ht_0 = Ht_{int}$, with: ρ_v= linear current density of Jv on Cv

The induced current distribution: Jv, is, also, an external current distribution induced by the internal distribution: Jp, on the contour Cv, with respect to the magnetic configuration inside Cv, but what happens inside the contour Cv? We will investigate this very particular case in the following section.

3.4. Generation of the magnetic configuration inside the Cv contour

We saw in the previous section (Figure 4) that the internal distribution: Jp, induces a current distribution on the external contour Cv. Let us look in detail at what happens inside Cv, contour on which we have placed a virtual shell. The current distribution: Jv, induced on Cv, satisfies the equation:

Equation 7: Relationship between *Jv* and *Jp*

$$\emptyset v = 0 \rightarrow MVV * Jv + MVP * Jp = 0$$

The current distribution Jv is an external current distribution, located on the contour Cv. According to § 3.2, it generates, alone on Cv, the internal magnetic configuration, initially created by all the conductors outside Cv. Equation 7 shows that the internal distribution: Jp, generates, on the external contour Cv, the induced external distribution: Jv. We have shown in § 3.3, that this distribution cancels the fields and fluxes, created by the distribution: Jp, on the contour Cv and outside Cv and that the only non-zero resulting tangent fields are the tangent fields inside Cv.

In reality, there is no virtual shell, so Equation 7 simply translates that the distribution: Jp, internal, cancels the fluxes generated by the distribution: Jv, on the contour Cv, thus maintaining the contour Cv zero-iso flux, in the presence of Jv. The distribution: Jp, canceling the fluxes on Cv, the opposite distribution: $-Jp$, therefore satisfies the internal fluxes and inside fields on the contour Cv. Thus, the distribution: $-Jp$, is the internal current distribution, the sought-after solution, which generates the magnetic configuration created by the external distribution: Jv, inside Cv. Indeed, we first placed the internal distribution: Jp, which "generates" on Cv the external distribution: Jv, then we add the internal solution: $-Jp$, which satisfies the internal fluxes and fields on the contour Cv. There is therefore no longer any internal current distribution on the contour Cp and the internal magnetic configuration inside Cv is entirely generated by the sole distribution: Jv, "induced" on Cv by the distribution: Jp.

As by definition the internal distribution generates the fields and fluxes inside Cv, the same rule applies to the sole internal distribution: J_{int}, located on Cp. Indeed, the distribution: Jp, which cancels the fluxes on Cv is equal to: $Jp = -J_{int}$; the distribution that satisfies the fluxes and fields on Cv is opposite: $-Jp$. Thus, there remains only the initial distribution J_{int}, on Cp, which generates the fluxes and fields located between the contours Cp and Cv.

We can conclude that the previous rule applies as well to an external distribution as to an internal distribution and that the only internal current distribution, located on the contour Cp, generates the fluxes and fields internal to Cv, therefore the magnetic configuration located between the contours Cp and Cv.

Finally, all the magnetic measurements intended for the evaluation of the internal Jp solution must be located on a single physical contour merged with the contour Cv, where the external current distribution is induced.

4. Plasma displacement analysis

4.1. Displacements of a rigid conductor in a magnetic field

The plasma displacement law is not the one we know when we move a rigid conductor (index D) carrying a constant current (Id) in an external magnetic field created by a set of external coils (index B). Indeed, in this case, the forced displacement of the conductor D generates a variation in the mutual inductance MBD between the conductor D and the contour of the coils B which in turn generates induced currents in the electrically closed coils according to Faraday's law:

$e = -d\emptyset/dt$, with: $d\emptyset/dt = Id * dMBD/dt$ (variation of the mutual with the displacement)

As the circuit of the coils is closed then the induced current: JB, in the outer coils are expressed by:

Equation 8: Current distribution induced by variation of mutual inductances

$$MBB * \frac{dJB}{dt} + Id * \frac{dMBD}{dt} = 0$$

The plasma is not a rigid conductor: it deforms and adapts to the external magnetic field without generating induced currents outside and inside its contour as it will be explained in the following section.

4.2. Virtual shell principle applied to plasma displacements

The principle of the virtual shell and its properties, described in § 2.2, constitute the key that will allow us to understand and establish a representative model of plasma movements. The virtual shell is superconducting, deformable at will and very thin.

As a reminder, the movements and deformations of a virtual shell in the presence of the external and internal magnetic configurations induce a distribution of currents in the thickness of the shell that does not modify the internal and external magnetic configurations (§2.2.3). In other words, during the movements of the shell, the external and internal magnetic configurations remain unchanged. There can therefore be no currents induced by the movements of the shell in the external coils or in the plasma section.

We will now consider the following steps with the notations of Figure 5. Let us first consider a plasma at equilibrium on the contour C1, then this contour is iso flux by definition. Let us imagine that a disturbance of the external or internal field of the plasma modifies the equilibrium of the plasma on C1 then, as the mechanical inertia of the plasma is zero (negligible mass) the latter moves instantly on another contour C2 in order to adapt to the existing external magnetic field and maintain its equilibrium on the new contour C2. The contour C1 is therefore no longer iso flux and flux deviations: $\boldsymbol{\Delta\emptyset}$, appear on the periphery of the contour C1.

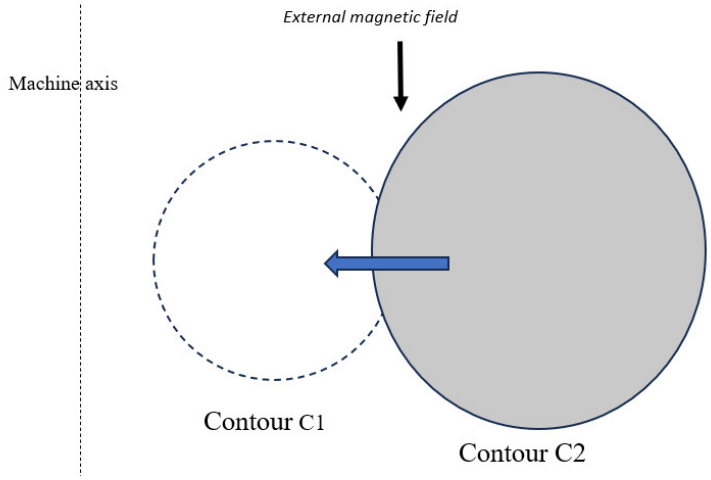

Figure 5

Now let us imagine that a virtual shell is placed on the contour C2 and then that this contour C2 is moved back to the contour C1. Then, a variation of the induced current distribution: JP_d, appears on the virtual shell during the movement from C2 to C1. It should be noted that the flux deviations: $\boldsymbol{\Delta\emptyset}$, on the contour C1, remained unchanged during the movement from C2 to C1 because the external (and internal) magnetic configuration remained unchanged (property of the virtual shell). The variation of the induced distribution: JP_d, only reflects the electromagnetic disturbance that gave rise to the plasma movements from C1 to C2, as we will see in the next step.

The plasma is now positioned on the C1 contour but with an induced variation of the: JP_d, distribution, present on the virtual shell. In order to be able to remove the virtual shell, it is first necessary to cancel the variation of the: JP_d, distribution on the virtual shell using the poloidal field coils according to the equation:

Equation 9: Cancellation of distribution: JP_d, by poloidal field coils on the contour C1

$$MPB * JB + MPP * JP_d = 0,$$

MPP and MPB are the matrices of the mutual inductances on C1 and between the contours C1 and Cp.

Indeed, it is a question of inducing a current distribution on the shell which cancels the distribution: JP_d. Thus, after the cancellation of the distribution: JP_d, the shell can be removed and the plasma is again at equilibrium on the contour C1. The flux differences on C1 have disappeared with the distribution: JP_d, which clearly shows that the variation of the current distribution: JP_d, "generates" the flux differences on the contour C1.

The current distribution: JP_d, is decomposed according to a so-called magnetizing distribution: JP_m, and a distribution: JP_e, at zero-ampere-turns. The magnetizing distribution is defined on the C1 contour of the plasma as generating a uniform flux on the C1 contour (iso flux):

$$MPP * JP_m = \emptyset P_m \text{ iso flux, with: } \sum JP_m = \sum JP_d$$

The distribution: JP_e, is therefore a distribution with zero-ampere-turns:

$$JP_e = JP_d - JP_m$$

The distribution: JP_m, reflects a change in the plasma flux but does not generate any flux deviation on C1 by definition of the magnetizing distribution. On the other hand, the distribution: JP_e, at zero-ampere-turns, represents the equivalent electromagnetic disturbance that gave rise to the plasma displacements. This distribution generates the flux deviations: $\boldsymbol{\Delta\emptyset}$, on the contour C1.

4.3. Modelling plasma displacements without virtual shell

The plasma displacements can therefore be modelled by a virtual current distribution: JP_e, at zero-ampere-turns, located on the fixed contour: C1, which satisfies the flux deviations on this contour. This distribution represents the external equivalent electromagnetic disturbance which generated the plasma displacements, from the contour C1 to another contour C2. For example, when the poloidal field coils generate a flux disturbance: $\boldsymbol{\Delta\emptyset}$, on the contour C1, the plasma moves instantaneously, revealing a virtual current distribution: JP_e, on C1, which satisfies these same flux deviations on C1. We showed in § 3.4. that the internal distribution Jp on the contour Cp, interior at C1, alone, generates the magnetic configuration inside the contour of the magnetic measurements. Thus, the expression of the flux deviations on C1: $\boldsymbol{\Delta\emptyset}$, is expressed in two ways: either with the external distribution: J_{ext}, at zero-ampere-turns, or with the internal distribution: JP_e, equivalent, with: $J_{ext} = JP_e$, on the contour C1.

Thus, recovering plasma equilibrium on C1 requires cancelling the flux deviations generated by this current distribution: J_{ext} or JP_e, on C1 using the poloidal field coils still according to Equation 9, but with the distribution: JP_e, instead of JP_d. As in reality, there is no virtual shell, this equation necessarily translates a cancellation of the flux deviations on the C1 contour, by the external coils as if the plasma did not exist.

During the movements of the plasma, an external observer only perceives the flux deviations appearing on the external contour C1, generated by an electromagnetic disturbance internal or external to the plasma. The equilibrium of the plasma therefore requires a permanent control of the flux on the C1 contour as if the plasma did not exist as a conductor. The plasma will therefore be ignored as an active conductor in the electromagnetic equations of the machine for the determination of the control loop of the plasma movements at constant plasma current: Ip.

5. Calculating the interior current distribution Jp satisfying the magnetic measurements

The following evaluation remains valid for a machine with or without a magnetic core because the plasma and the vacuum chamber are located in air or vacuum (relative magnetic permeability: μr =1).

5.1. Problem position

We have shown in § 3.4, that the only interior distribution Jp located on the contour Cp, interior to the measurement contour Cm, generates the magnetic configuration in the space located between the contour Cp and the contour Cm.

We are therefore looking for the interior current distribution: Jp, on the contour Cp, located inside the plasma contour C1, which satisfies the field and flux measurements on the contour Cm, according to Figure 6.

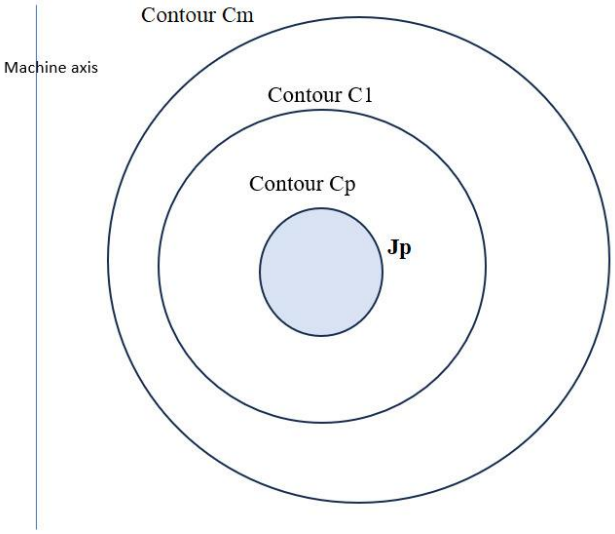

Figure 6: Contour arrangement with the Cp contour located inside all the plasma contours

As the number of real field and flux measurements is limited: Nf flux measurements and Nh field measurements, we will determine the internal current distribution Jp, which best satisfies a larger number of measurements: Nc, such that: Nc >> Nf and Nc >>Nh but which exactly satisfies the flux and field measurements on the real measurement points.

In fact, knowing the fluxes is enough to determine the internal distribution Jp. The fields are therefore redundant measurements. The general problem then boils down to the compromise solution simultaneously minimizing the flux errors and the field errors at the level of the measurement contour for a common current distribution Jp located on a contour interior to the plasma contour C1.

Let Q_F be the quadratic function to be minimized for the fluxes and Q_H the one for the fields. Simultaneously minimizing the two functions amounts to minimizing the function:

$$Q = \gamma * Q_F + \alpha * Q_H, \text{ with } \alpha \text{ and } \gamma \text{: any positive real numbers.}$$

In this form it is possible to easily calculate the solution exclusively with the fields (γ=0) or exclusively with the flux (α =0) and of course, the mixed solution with the field and flux measurements.

5.2. Reminder on optimization under equality constraint

Let: $F(x_{1,}x_{2,}\ldots.,x_{n,})$, a function of N variables to be optimized under the equality constraint defined by: $f(x_{1,}x_{2,}\ldots.,x_{n,})$=0.

Ignoring the constraint initially, the conditions necessary at first order, for the optimization of the function F, are expressed by: $dF = 0$, i.e. N simultaneous conditions:

$$\frac{\partial F}{\partial x_1} = 0, \qquad \frac{\partial F}{\partial x_2} = 0, \ldots \quad \ldots \frac{\partial F}{\partial x_n} = 0,$$

To take the constraint into account, the mathematician J.L. Lagrange's trick (LAGRANGE, 1788) is to differentiate the function: $F + \lambda f$, where: $f = 0$, is the differentiable constraint, i.e. the true relation whatever the value of λ:

$$\left(\frac{\partial F}{\partial x_1} + \lambda \frac{\partial f}{\partial x_1}\right) dx_1 + \left(\frac{\partial F}{\partial x_2} + \lambda \frac{\partial f}{\partial x_2}\right) dx_2 + \cdots \left(\frac{\partial F}{\partial x_n} + \lambda \frac{\partial f}{\partial x_1}\right) dx_n = 0.$$

Then he imposes the value of λ, such that:

$$\frac{\partial F}{\partial x_n} + \lambda \frac{\partial f}{\partial x_n} = 0.$$

From this step, he demonstrates that minimizing the function F under the constraint of equality: $f = 0$, amounts to minimizing the function: $F + \lambda f$, in a constraint-free system with N equations, but with N+1 variables, in adding λ to it and where the N+1st equation is simply the constraint itself.

Adding more constraints is resolved in the same way with new values of λ from λ_1 to λ_k, associated with the condition of equality of rank differentials: $N - k + 1$.

5.3. Solving the problem in a free system therefore without constraint

We will first solve the problem in a free system, therefore without constraints, of Np variables: the current distribution: Jp, located on the interior contour Cp.

The quadratic function: Q_F, is defined by: $Q_F = \sum_{i=1}^{Nc_f} {\varepsilon_F}^2$ and $\varepsilon_F = MCP * Jp - \emptyset c$, with:

- Nc_F = number of flux measurement points including real measurements but also fictitious additional measurements,
- MCP, the matrix of mutual inductances of the fluxes between the distribution Jp and the points on the measurement contour,
- $\emptyset c$, the distribution of fluxes on the points of the measurement contour.

Thus, the optimization of Q_F will result in: $dQ_F = 0$, namely, Np equations which are expressed in matrix form by: ${}^T MCP * \varepsilon_F = 0$.

In the same way, the optimization of the function: Q_H, will result in the matrix equation: ${}^T HCP * \varepsilon_H = 0$, where: HCP is the matrix expressing the tangent fields as a function of the current distribution Jp on Nc_H field measurement points greater than the actual number of real measurements.

Finally, the overall problem boils down to the equation:

$$\gamma * {}^T MCP * \varepsilon_F + \alpha * {}^T HCP * \varepsilon_H = 0.$$

By replacing ε_F and ε_H, by their original expressions, we obtain:

$$\gamma * {}^T MCP * [MCP * Jp - \emptyset c] + \alpha * {}^T HCP * [HCP * Jp - Hc] = 0, \text{ which is written:}$$

$$\left[\gamma * {}^T MCP * MCP + \alpha * {}^T HCP * HCP\right] * Jp = \gamma * {}^T MCP * \emptyset c + \alpha * {}^T HCP * Hc$$

By introducing a current smoothing function of Jp which minimizes the sum of the squares of the currents $Jp(i)$ we obtain the final matrix to be inverted QPP:

$$QPP = \left[\gamma * {}^T MCP * MCP + \alpha * {}^T HCP * HCP + \beta * Ipp\right],$$

where: Ipp is the identity matrix NpxNp and β, a positive number as small as possible.

Finally, the current distribution: Jp, a solution which best satisfies the fluxes and the tangential fields on the measurement contour Cm, is expressed by:

Equation 10: Expression of Jp versus the magnetic measurements

$$Jp = \gamma * QPP^{-1} * {}^T MCP * \emptyset c + \alpha * QPP^{-1} * {}^T HCP * Hc, \text{ written:}$$

$$Jp = FPC * \emptyset c + BPC * Hc$$

with: $FPC = \gamma * QPP^{-1} * {}^T MCP$ and $BPC = \alpha * QPP^{-1} * {}^T HCP$

The Jp solution does exist but it is expressed according to real measurements and also fictitious measurements. In order to determine the solution Jp, expressed solely as a function of the real measurements, it is necessary to add constraints to the

previous free system by forcing the solution Jp to exactly satisfy the fluxes and fields at the level of the real measurements, i.e.: Nf + Nh constraints.

5.4. Solving the final problem with multiple constraints

In order to solve this problem as simply as possible we will use the Lagrange multiplier method which amounts to solving the problem in a system free of constraints but this time with: Np+Nh+Nf variables where the Nh+Nf additional variables are the values ƛ(i) of the Lagrange multiplier associated with each constraint. The Nh + Nf linear constraints represent the additional equations to solve the global free system.

In the present case, the constraints are already implicitly integrated into the equations of the previous free system in the form of the measurement error: ε_F or ε_H, associated with the real measurements. So, rather than introducing the constraints in linear form: ε_F=0 and $\varepsilon_H = 0$, for each real measurement, we will define the differentiable functions associated with the constraint by their quadratic forms: ε_F^2 =0 and ε_H^2 =0. In this way, we can simply show (§7.2.2) that the values of ƛ, Lagrange multiplier, are carried over to infinity for all constraints, which does not require solving the additional Nh+Nf equations which are implicitly solved for very large values of ƛ.

To solve this system with Nh+Nf constraints, it suffices to modify the matrices: ${}^TMCP$ and ${}^THCP$, by the following respective matrices: ${}^TM0CP$ and ${}^TH0CP$, where all columns whose index corresponds to a real measurement are multiplied by: 1+ ƛ, in each of the two matrices.

The solution is always defined by Equation 10, where, the matrices: ${}^TMCP$ and ${}^THCP$, are replaced by the respective matrices: ${}^TM0CP$ and ${}^TH0CP$, with ƛ very large. At this stage, we still have the fictitious measurements on the contour Cc, but their contribution to the distribution Jp solution is now zero, for ƛ very large in the case of the system with constraints. We can now restrict the FPC and BPC matrices to only real measurements, i.e. Nf flux measurements and Nh field measurements. Let: $F0PC$ and $B0PC$ be the restricted matrices of respective dimensions: NpxNf and NpxNh, where Nf and Nh are the numbers of respective real measurements of flux and fields.

There you have it, we have determined our solution: Jp, which exactly satisfies the real flux and field measurements located on the measurement contour Cm.

5.5. The zero-amperes-turns solution JPe, which generates the flux differences on C1

The final solution at zero-ampere-turns which satisfies the flux deviations on the fixed contour C1 is expressed by:

$$Jp_e = Jp - Jp_m$$

where: Jp_m, is the internal magnetizing distribution on the contour C1, defined by:

$M1P * Jp_m$=$\emptyset 1_m$, iso flux on C1 and $\sum Jp = \sum Jp_m$

In reality we do not need to calculate the current distribution: Jp_m, to evaluate the flux differences on C1 because the latter are defined by differential fluxes where the common flux component does not intervene. We will therefore calculate the fluxes on C1 directly with the solution Jp then the flux differences:

Equation 11: Expression of flux deviations on C1 using the solution: Jp

$$\emptyset 1 = M1P * Jp \rightarrow \Delta\emptyset(i) = \emptyset 1(i) - \emptyset 1(1), \text{ for i=1 to N1.}$$

5.6. Plasma current evaluation using the Jp solution

The internal distribution Jp that satisfies the magnetic measurements must be used to calculate the amplitude of the plasma current in real time by summing the ampere-turns

$$Ip = \sum_1^{Np} Jp(i), \text{ for: i=1 to Np.}$$

The value of Ip, thus calculated, is very accurate, therefore, the approximate calculation of the circulation of the tangent field along the measurement contour is no longer necessary.

5.7. Numerical evaluation of the Jp solution

In order to corroborate the previous calculations with reality, the numerical application was carried out with data from the TORE SUPRA (WEST version) machine, located in Cadarache (France), including:

- The spatial coordinates of tangent field and flux measurements, practically located on the same contour.
- A total number: Nf=6, of flux measurements distributed over the contour,
- A total number: Nh=51, of tangent field measurements distributed over the contour.

Figure 7 shows the distribution of measurements on the Cm contour and the Cp contour carrying the current distribution.

In order to control the convergence of the solution, we placed a constant current distribution on the Cp contour which generates the measurements on the Cm contour. Next, the converging program returns a current distribution that must match the input value. This test makes it possible to easily adjust the program parameters, mainly the current smoothing parameter β and λ, the value of the Lagrange multiplier.

The results show that mixed measurements make convergence narrow. In this specific case, the currents generated respectively by the fields and the fluxes are antagonistic and of significant amplitude. In addition, there is the presence of harmonic currents which make convergence more delicate but after convergence the precision is correct.

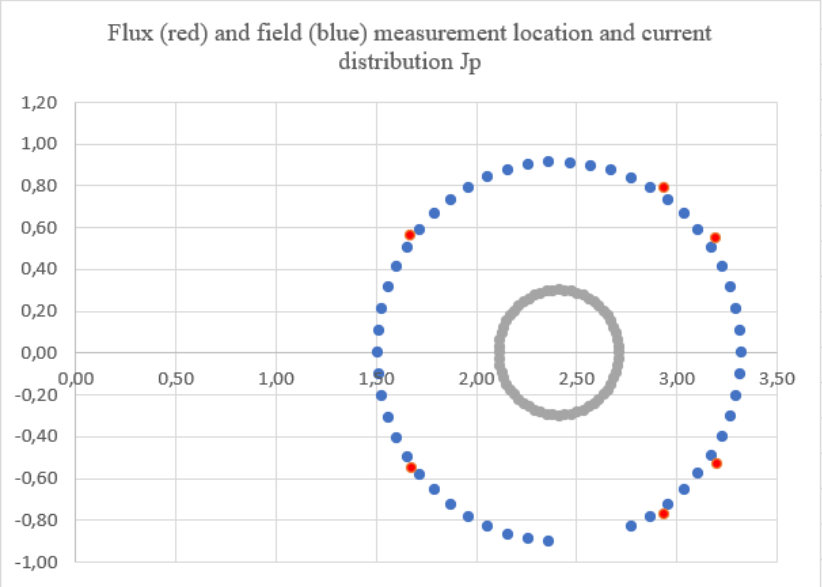

Figure 7: Measurement points on Cm and internal contour Cp

By using only flux measurements (parameter α =0), the convergence is easy but the precision is simply lacking because of the reduced number of flux measurements (Nf=6).

By using only field measurements (parameter γ=0), the convergence is excellent and the precision excellent, from 14 to 51 tangent field measurements regularly distributed over the contour.

All the previous solutions return an extremely precise amperes-turns value unlike the calculation of the circulation of fields on the measurement contour.

6. Magnetic measurements

All calculation results presented in this section were carried out using the general solution: Jp, developed in § 5.

6.1. Introduction

Magnetic field and flux measurements are installed inside the vacuum chamber containing the plasma in order to reconstruct the flux distribution on the assumed plasma contour C1 as well as to evaluate the amplitude of the plasma current.

At the origin of Tokamaks in the early 1950s, the evaluation of fluxes on the assumed plasma contour was carried out thanks to a limited development of the flux, to the first order, using mixed measurements: flux and magnetic fields, positioned on the measurement contour. The plasma current was then evaluated by calculating the circulation of the tangent field along the measurement contour. Subsequently, this method was improved but still remains inaccurate when the plasma boundary moves away from the measurement contour.

Today, we have the possibility of calculating the distribution: Jp, interior, which satisfies the fluxes and fields on the measurement contour. We have shown in § 3.4, that the only internal solution: Jp, located on the contour Cp, generates the fields and fluxes in the space between the contour Cp, interior and the contour of measurements Cm. We will see that this method is flexible, extremely precise and allows to calculate the fluxes on the presumed contour of the plasma as well as the amplitude of the plasma current with an extraordinary precision. The downside with this method is that the use of mixed measurements imposes the constraint of positioning the field and flux measurements, on the same and unique physical contour.

6.2. Constraint of using the internal solution Jp with mixed measurements

We saw in § 3.4, that the magnetic measurements must be located on the same and unique regular physical contour because the solution Jp depends on the spatial position of the measurement contour. The use of measurements of the same type, flux or field, allows to overcome this constraint whereas with mixed measurements, the contour of the field measurements and that of the flux measurements can be different although close to each other.

In the case where some measurement points are not located on the measurement contour without being too far from the contour Cm, it is possible to approximate these measurements according to the measurements on Cm, and vice versa, using limited developments to the first order. It is then necessary to define a regular contour: Cm, with as little curvature as possible which passes through the field measurements. Indeed, it will subsequently be a question of expressing, if possible, all the fictitious flux measurements located on this contour Cm as a function of the real measurements, located nearby, thanks to a development limited to the first order. This requires that each real flux measurement close to the contour Cm be located on the normal to the contour Cm passing through a real field measurement on Cm.

6.3. What measurements with the Jp solution for good theoretical precision

We have seen that the mixed measurements must be located on the same physical contour, but in general this is not the case and it is necessary to fit the flux measurements located near the contour of the field measurements, using first-order limited expansions. Moreover, the Jp solution calculated with the mixed measurements is not easily convergent because the part of the Jp distribution generated by the fields and that generated by the fluxes are opposite and of large amplitude, with on the other hand the presence of harmonics of currents superimposed with the solution, leading to a tight convergence. Therefore, using single type measurements avoid the problems encountered with mixed measurements and provide good results.

Flux measurements are sufficient to evaluate the interior: Jp, solution; tangent field measurements are therefore redundant measurements.

It is shown numerically that, at least, twelve measurements (without redundancy) of tangent fields or absolute fluxes are sufficient to calculate the Jp solution with very good accuracy, for small machines as well as for large machines such as ITER or DEMO. The necessary and sufficient conditions for obtaining correct results are:

- A uniform distribution of field or flux measurements, along the measurement contour, whether fictitious or real,
- A measurement contour that is as regular as possible with the lowest required curvature,
- A sufficient number of fictitious measurements of the same type, in addition to the real measurements, on which the exact measurement constraints are applied (see § 5.4).

Finally, the greater the number of real measurements, the better the accuracy is for evaluating the Jp solution. In short, a number of field or flux measurements between 12 and 30 is suitable for good precision of the Jp distribution. In general, the returned ampere-turns are returned with a relative precision of less than 10^{-6}. Calculations show that the local values: $Jp(i)$, are affected by a lower precision than that obtained on the total ampere-turns by the presence of harmonic currents

whose amplitude decreases with the number of real measurements of the same type. Despite everything, the difference between 12 and 30 measurements is not significant.

However, in the event of a measurement loop failure, the accuracy deteriorates in the first inner third of the measurement contour (§ 6.8) and it is necessary, in this case:

- To increase the minimum number of measurements, not by 1 but by 2 to 4 additional measurements,
- To concentrate more measurements in the first inner third of the measurement contour and to maintain, or even partially reduce, the number of measurements regularly distributed in the outer 2/3 of the measurement contour.

6.4. What measurements for the reliability of plasma control

Concerning the numerical results, with flux measurements or field measurements, the precision of the calculations is equivalent for the same number of measurements of the same type. The only difference between these two types of measurements lies in the much higher signal level for absolute flux measurements than for tangent field measurements. In an environment polluted by parasitic and permanent electromagnetic sources, it is clear that the priority goes to the use of absolute flux measurements which are, moreover, directly usable in the calculations unlike differential flux measurements. The only challenge concerning the measurements in general concerns the drift of the integrators over long cycle durations with plasma, but which is lower for fluxes than for fields, with higher signal levels therefore with lower integral gains than for fields.

6.5. Numerical confirmation with only flux measurements without redundancy

We propose to numerically show the efficiency of flux measurements for evaluating the interior Jp solution, in the case of a virtual machine, larger than the ITER Tokamak,

6.6. Virtual machine geometric data

In this virtual machine, the measurement contour Cm and that of the current distribution Cp were modelled by elliptic curves comprising 60 to 70 fictitious and real measurement points for the measurement contour Cm and 60 conductors for the contour Cp.

Contours parameters		
Large radius Cm contour (m)	R0	9,66
Small radius Cm contour (m)	R1	3,64
Number of flux points	Nm	60 to 70
Large radius Cp contour (m)	r0	9,66
Small radius Cp contour (m)	r1	1,2
Number of conductors	Np	60
Eccentricity	Ex	2
Homothety factor	Hx	4

Table 1: Geometric data of the virtual machine

This virtual machine was obtained from the configuration of the TORE SUPRA machine WEST version, thanks to a homothety of a factor: 4 and an eccentricity of a factor of 2 for the elliptic shapes. The geometric data of the virtual machine are summarized in Table 1.

The following figure shows the contours Cm and Cp in a vertical plane passing through the machine axis. All dimensions are given in meters (m).

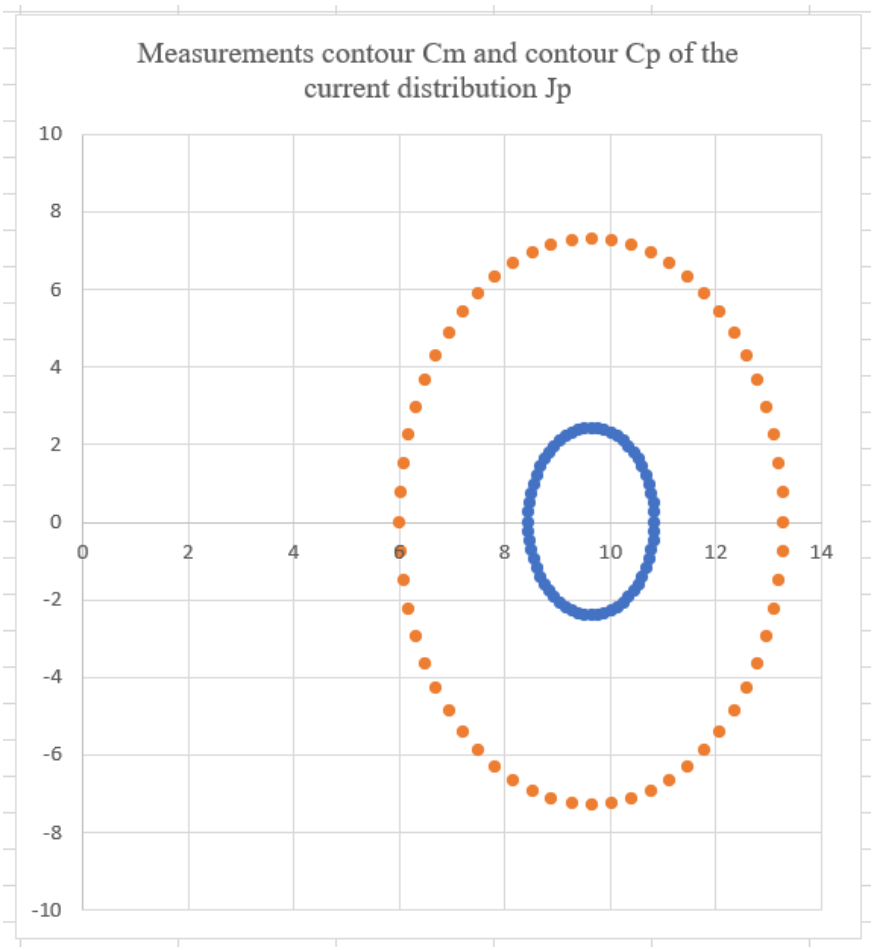

Figure 8: Contour Cm and Cp in the large virtual machine

6.7. Numerical results

The calculation of the solution Jp satisfying the flux measurements located on the contour Cm was carried out according to the number of real flux measurements, ranging from 6 measurements to 30 flux measurements, regularly distributed on the contour Cm, thanks to the general solution Jp, developed in § 5.

The convergence test consists of placing an initial distribution at constant current of 6000A, carried by 60 elementary conductors (100A per conductor) which generates the fluxes on the measurement contour Cm and which the converging program must restore. Convergence is ensured by the proper choice of the value of the Lagrange multiplier (Lambda) and thanks to the increasing adaptation of the smoothing coefficient of the current distribution Jp (Beta). Figure 11 shows the distribution Jp(i) returned by the converging program according to two distinct scales in order to assess the relative precision on the distribution Jp(i).

The following Table 2 summarizes the results of the numerical simulations carried out according to the number of real flux measurements, from 6 to 30 measurements.

The parameters « Lambda » and « Beta » are the convergence parameters of the solution Jp:

- « Lambda » is the Lagrange multiplier carried to infinity (10^{+9}),
- « Beta » is the smoothing parameter of the current distribution Jp.

This table shows the relative precision obtained on the distribution Jp(i) and that obtained on the ampere-turns: Ip. The curves in Figure 9 and Figure 10 respectively describe the evolution of the relative precision on the distribution Jp(i) and that of the ampere-turns Ip according to the number of flux measurements.

Number of real flux loops	Total number of measurements	Jp(i) accuracy	Ip accuracy	Lamda	Beta
6	60	8,00E-03	2,30E-05	1,00E+09	5,00E-05
8	64	5,00E-03	1,00E-05	1,00E+09	3,00E-05
10	60	2,00E-03	1,40E-06	1,00E+09	1,00E-05
12	60	1,00E-03	4,00E-07	1,00E+09	5,00E-06
15	60	4,00E-04	1,90E-07	1,00E+09	5,00E-06
17	68	2,00E-04	2,90E-07	1,00E+09	1,00E-05
20	60	8,00E-05	1,00E-06	1,00E+09	5,00E-05
25	50	3,00E-05	2,00E-07	1,00E+09	1,00E-05
30	60	4,00E-05	3,20E-07	1,00E+09	2,00E-05

Table 2: Results of the simulations according to the measurement number

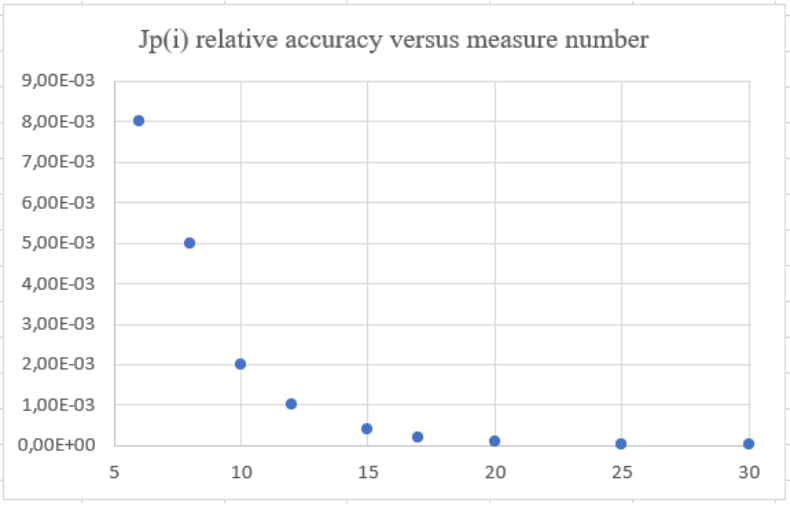

Figure 9: Relative accuracy on the distribution Jp as a function of the number of measurements

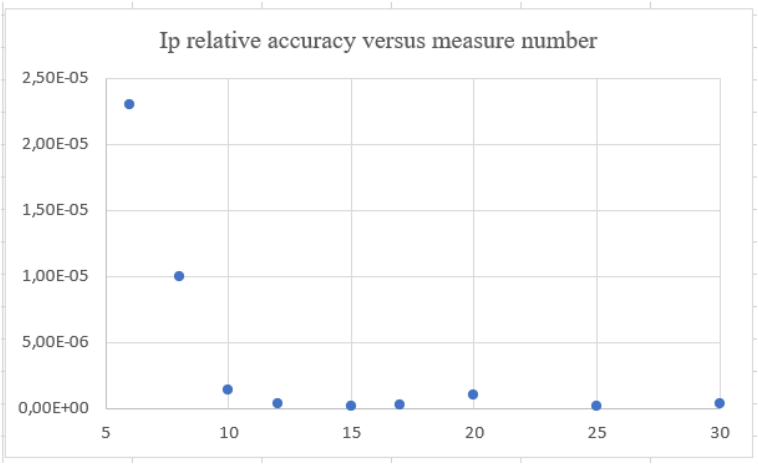

Figure 10: Relative accuracy on ampere-turns Ip as a function of the number of measurements

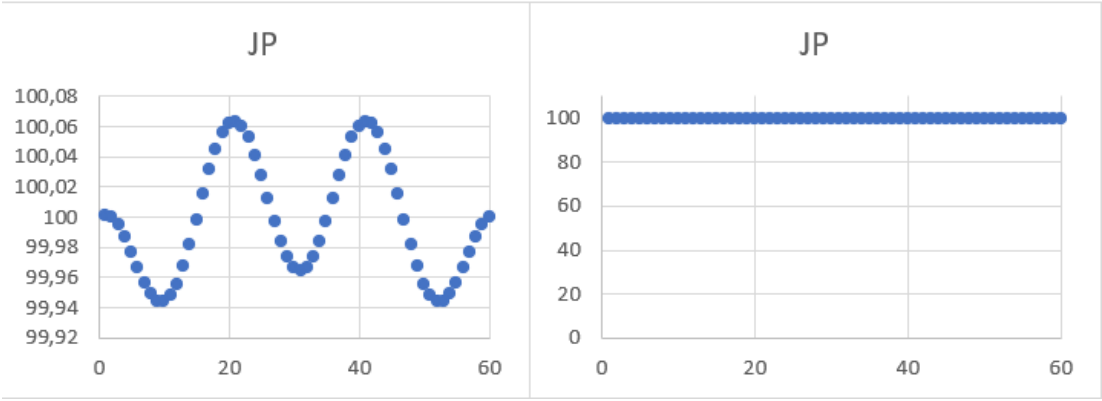

Figure 11: Values of Jp returned by program for 15 flux measurements

6.8. Redundancy: case of one faulty measurement among 15 measurements

We assume that 15 real flux measurements (60 measurements in total including fictitious measurements) are positioned and equally distributed on the contour Cm. We will then calculate the solution Jp and the relative associated errors on Jp(i) and Ip, assuming one defective measurement among the 15 existing measurements and investigate the influence of the position of the defective measurement on the relative accuracy of the Jp distribution.

Point: 1, is the innermost point (closest to the machine axis); the numbering from 1 to 60 proceeds clockwise with a regular distribution of the measurements.

Table 3 summarizes the simulation results. Figure 12 shows the relative precision on Jp(i) and Figure 13, that of the plasma current, versus the position of the failed loop.

The accuracy obtained with 15 valid measurements is 5.0 10^{-4} on Jp(i) and 7.3 10^{-8} on Ip.

Number of real flux loops	Failed loop position	Jp(i) accuracy	Ip accuracy	Lamda	Beta
15/60	no failed loop	5,00E-04	7,30E-08	1,00E+09	1,00E-06
15/60	1	5,00E-03	5,50E-06	1,00E+09	5,00E-07
15/60	5	2,50E-03	1,80E-06	1,00E+09	1,00E-06
15/60	9	4,50E-04	2,30E-07	1,00E+09	5,00E-06
15/60	13	5,00E-04	2,30E-07	1,00E+09	5,00E-06
15/60	17	5,00E-04	2,30E-07	1,00E+09	5,00E-06
15/60	21	5,00E-04	2,30E-07	1,00E+09	5,00E-06
15/60	25	5,00E-04	2,30E-07	1,00E+09	5,00E-06
15/60	29	5,00E-04	2,30E-07	1,00E+09	5,00E-06
15/60	33	7,00E-04	5,00E-07	1,00E+09	1,00E-05
15/60	37	5,00E-04	4,30E-07	1,00E+09	1,00E-05
15/60	41	5,00E-04	4,30E-07	1,00E+09	1,00E-05
15/60	45	5,00E-04	4,30E-07	1,00E+09	1,00E-05
15/60	49	5,00E-04	4,30E-07	1,00E+09	1,00E-05
15/60	53	5,00E-04	1,60E-07	1,00E+09	1,00E-06
15/60	57	3,00E-03	3,00E-06	1,00E+09	1,00E-05

Table 3: Simulation results depending on the position of the faulty loop

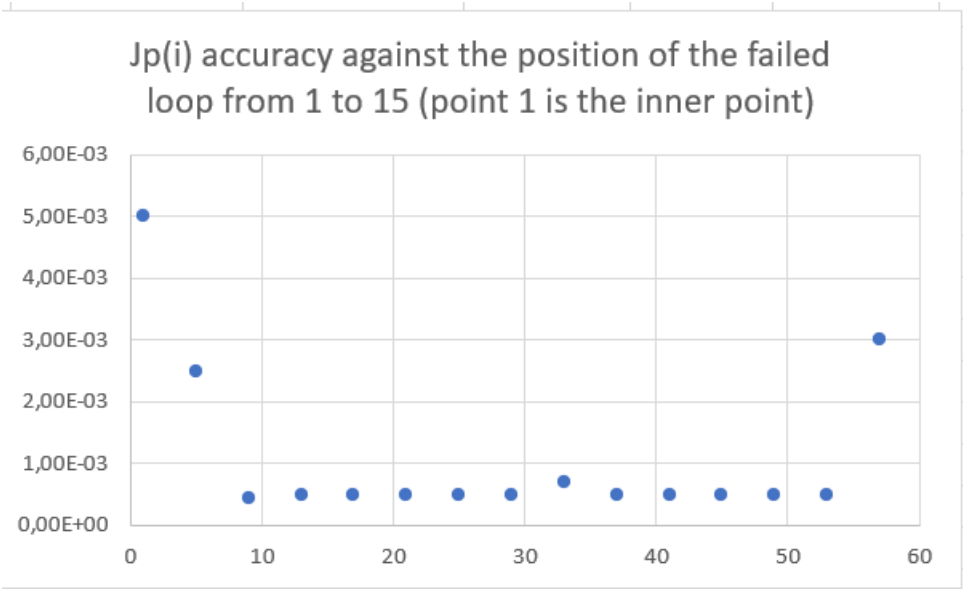

Figure 12: Relative precision on Jp(i) versus the position of the failed loop

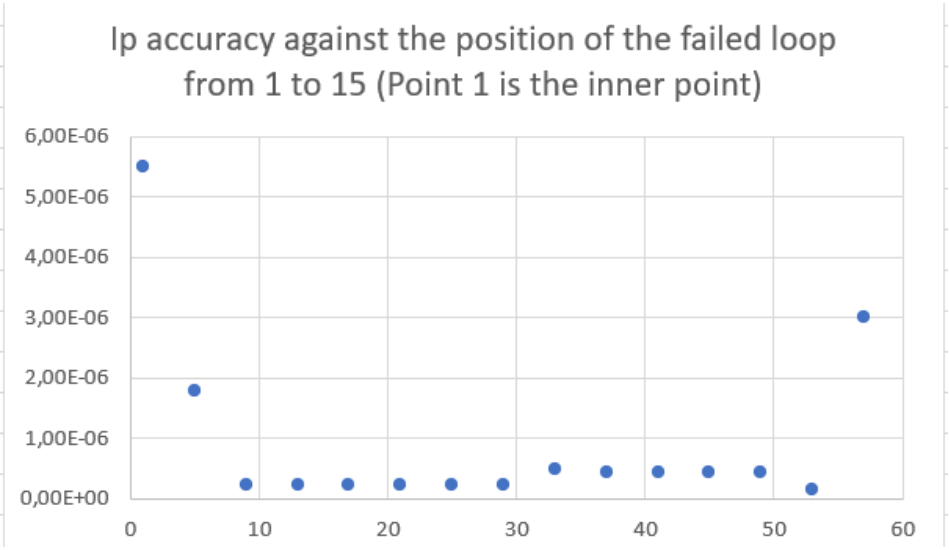

Figure 13: Relative precision on Ip versus the position of the failed loop

The results show that the accuracy depends on the measurement position. The first third of the measurements from point:1, the innermost, is strongly affected by a lower accuracy (5 to 10 times lower) while the other outermost points are little or not affected.

Thus, the tendency would be rather to concentrate more measurements on the first inner third than on the rest of the contour rather than a regular distribution as recommended.

6.9. Conclusion on the numerical results obtained

The minimum number of measurements, necessary for the evaluation of the solution Jp, must be at least equal to 12 regularly distributed measurements, according to Figure 10 and without redundancy.

Beyond 12 measurements, there is practically no difference, because the contribution of fictitious measurements is almost non-existent in all cases with more than 12 real measurements. We saw in § 5.4 that the adaptation of the Lagrange multiplier fixed at a sufficiently large value, makes it possible to annihilate the influence of fictitious measurements. Thus, the sum of the columns associated with the fictitious measurements of the FPC matrix expressing the current distribution

Jp as a function of the real and fictitious measurements, is almost zero for all fictitious measurements; which makes it possible to restrict the FPC matrix to real measurements only.

The study of § 6.8 on the influence of a defective measurement among 15 measurements would rather show that it is necessary to place more measurements on the first inner third of the contour and to maintain or reduce the concentration of measurements on the remaining 2/3.

7. Evaluation of the plasma control loop

In this section, the plasma boundary is assumed to be a constrained boundary, located on the fixed C1 contour.

7.1. Problem position

The plasma position control loop aims to maintain a permanent iso-flux distribution on the presumed C1 contour of the plasma. As mentioned in § 4.3, the plasma is completely ignored as an active conductor, because it is indeed a flux control on the C1 contour, carried out using poloidal field coils; which leads us to determine the solution Jb which best satisfies the fluxes on C1.

More precisely, we wish to control the fluxes as best as possible on Np points of the C1 contour, with $Np \geq Nb$, or even exactly on one to Nb points of the C1 contour, by increasing the number of constraints. It is clear that we can only exactly control up to Nb flux points on C1 using the poloidal field coils, but only one constraint is necessary: an exact flux at a single point, chosen as the reference point of the fluxes on the C1 contour, for example the inner point of the plasma in contact with the inner limiter or other. This point is the reference point for calculating the flux deviations.

The use of a number of constraints lower than Nb offers the possibility of optimizing the poloidal coil currents, which is not possible with Nb constraints. In a machine without a magnetic circuit, the solution: Jb, determines the evolution, therefore the amplitude, of the coil currents from the plasma current generation phase until the end of the cycle

Furthermore, the calculation of the fluxes on a larger number of points on C1 (Np > Nb) does not pose a problem thanks to the knowledge of the distribution: Jp, which exactly satisfied the magnetic measurements on the contour Cm, exterior to the plasma (§ 5).

7.2. The main Jb solution satisfying the flux on C1

The solution: Jb, is objectively the solution which satisfies at best the fluxes on Np points (with: $Np \geq Nb$) of the contour C1, i.e. the solution: Jb, first defined by:

$$\emptyset P = MPB * Jb.$$

In other words, we seek the opposite solution: Jb, which is expressed as a function of the Np (or N1) flux values on C1 (or Cp) by:

$$Jb = KBP * \emptyset P,$$

where KBP is the matrix to be determined, with: $Np \geq Nb$.

It results that the matrix product: $KBP * MPB$, is numerically very close to the identity matrix: Ibb which dimensions are NbxNb.

Equation 12: property of the KBP matrix

$$KBP * MPB \sim Ibb, \text{ of dimensions: NbxNb, for: } Np \geq Nb$$

We assume, in this calculation, that the machine does not have a magnetic core; we will show in § 8 that the control of plasma movements, carried out with the fluxes of the coils rather than the currents, adapts easily and without change to a machine with a magnetic core.

The influence of the vacuum chamber will be ignored in this calculation because the chamber is a passive structure. Flux control on C1 is achieved only by the poloidal field coils.

In order to find the Jb solution with constraints, we will use the Lagrange multiplier method to solve the system as already explained in § 5.2. The solution consists of first solving the problem without constraints and then adding one up to Nb constraints.

7.2.1. Solution Jb without constraint

The solution for a system free of constraint amounts to optimizing the flux differences: ε, on Np points of the plasma contour (Cp), with $Np \geq Nb$, which results in the function:

$$Q = \sum_{i=1}^{Np} \varepsilon(i)^2, \text{ where: } \varepsilon = \emptyset P - MPB * JB, \text{ with:}$$

- ε and ∅P are column vectors of dimensions Npx1 and
- MPB is the matrix of mutual inductances of dimension NpxNb, between coils and plasma contour.

Thus, minimizing the function Q results in the following Nb equations:

$$dQ = 0 => \frac{\partial Q}{\partial JB(j)} = 0, \text{ for: j=1 to Nb, with: } \frac{\partial Q}{\partial JB(j)} = \sum_{i=1}^{i=Np} \varepsilon(i) * MPB(i,j)$$

Either in matrix form: $${}^{T}MPB * \varepsilon = 0$$

Replacing ε, by its original expression leads to:

$${}^{T}MPB * [\emptyset P - MPB * JB] = 0 \rightarrow {}^{T}MPB * MPB * JB = {}^{T}MPB * \emptyset P$$

After introducing a coil current smoothing function where β is a real number as small as possible and Ibb, the identity matrix NbxNb, for cases with less than Nb constraints:

$$JB = \left[{}^{T}MPB * MPB + \beta * Ibb\right]^{-1} * {}^{T}MPB * \emptyset P$$

Thus, the matrix KBP which expresses Jb as a function of the fluxes on the contour C1 is:

Equation 13: Expression of the KBP matrix

$$JB = KBP * \emptyset P \rightarrow KBP = \left[{}^{T}MPB * MPB + \beta * Ibb\right]^{-1} * {}^{T}MPB$$

7.2.2. Adding constraints to the Jb solution

We will then solve the system with one linear constraint: $g = 0$, the necessary one which requires an exact flux: $\emptyset P(1)$, at the reference point on C1, which is expressed by:

$$g = \varepsilon(1) = \emptyset P(1) - \sum_{j=1}^{Nb} MPB(1,j) * JB(j) = 0.$$

The general method based on the Lagrange multiplier results in the optimization in a free system of Nb +1 equations, of the global function defined by:

$$Q + \lambda g, \text{ where } g = 0, \text{ is the differentiable constraint and } \lambda, \text{ a real number.}$$

Instead of using the linear constraint we will intentionally define the function g in the quadratic form of the error $\varepsilon(1)$ as:

$$g = \frac{\varepsilon(1)^2}{2} = 0$$

which will simplify the calculation of the value of λ which, in this case, is carried over to infinity as explained below.

Let us calculate:

$$d(\lambda * g) = 0 \longrightarrow \lambda * \varepsilon(1) * MPB(1,j) = 0, \text{ for j=1 to Nb}$$

where: λ is chosen such as:

$$\frac{\partial Q}{\partial JB(Nb)} + \lambda * \frac{\partial g}{\partial JB(Nb)} = 0$$

either again:

$$\frac{1}{1+\lambda} * \sum_{i=2}^{Np} \varepsilon(i) * MPB(i, Nb) = -\varepsilon(1) * MPB(1, Nb).$$

As the error: ε(1), must be zero while the other values of ε(i), are not, it is clear that the solution for λ is: $\lambda = \pm \infty$ which ensures: ε(1) =0.

The Jb solution including the constraint is always expressed according to Equation 13, where the matrix: ${}^{T}MPB$ is replaced by the matrix: ${}^{T}M0PB$, obtained by multiplying column 1 of matrix: ${}^{T}MPB$, by $1+\lambda$, with λ, a large positive real number:

$$JB = KBP * \emptyset P \rightarrow KBP = \left[{}^{T}M0PB * MPB + \beta * Ibb \right]^{-1} * {}^{T}M0PB$$

In this way, we can easily add up to Nb constraints and compare the solutions.

7.2.3. Expression of the optimal solution JBe

The general solution is expressed according to the relation: $JB_{opt} = KBP * \emptyset P$, with KBP the NbxNp matrix calculated previously. The breakdown of the column vector: $\emptyset P$, according to the differential fluxes on Np points, relative to the point: i=1, of the contour C1 is expressed by:

$\emptyset P(i) = \Delta\emptyset P(i) + \emptyset P(1)$, for i=1 to Np, where: $\Delta\emptyset P(1) = 0$

We therefore deduce the "magnetizing" component of current according to the flux: ∅P(1) at point 1, and the distribution of currents, associated with the differential fluxes: $\Delta\emptyset P(i)$, for i=2 at Np:

$JB_m(i) = \emptyset P(1) * \sum_{j=1}^{Np} KBP(i,j)$, for i = 1 *to* Nb, and:

$JBe(i) = \sum_{j=2}^{Np} KBP(i,j) * \Delta\emptyset P(j)$, for i=1 to Nb

As $\Delta\emptyset P(1) = 0$, by definition, the JBe solution is expressed as follows:

Equation 14: Expression of JBe, used for the plasma displacement control

$JBe = \widehat{KBP} * \Delta\emptyset P$, for i=1 to Nb and j=1 to Np-1, where:

$\widehat{KBP}(Nb, Np-1)$, is part of the matrix KBP in which the first column has been cancelled.

The JBe solution is the JB solution which will be used for the plasma displacement control loop.

In the rest of the document, we will continue to use the original KBP matrix, of rank Np, instead of $\widehat{KBP}$, despite the lower rank of the matrix for practical reasons including in particular the change of the reference point.

7.3. Comparison of the solutions in a virtual machine

In order to calculate and then verify the Jb solutions we defined a virtual machine and arbitrarily chose Nb=11 coils distributed on the exterior contour Cb. The central coil is numbered N° 1 and the other coils from: 2 to 11, are defined by turning clockwise from the inside:1. The Figure 14 below shows the geometry of the used contours including the coil contour Cb, the vacuum chamber Cc and the plasma contour C1 (or Cp).

To check and compare the solutions, we calculated the magnetizing distribution: JB_m, of the poloidal field coils from 1 to 11, for 1 Wb of constant flux, then we calculated the distribution of the magnetizing flux generated by this distribution on the contour C1, on Np=45 points of the C1 contour including the interior point 1, turning clockwise from the central point 1. This distribution of magnetizing current for 1 Wb of plasma flux is deduced from the KBP matrix (see § 7.2.3).

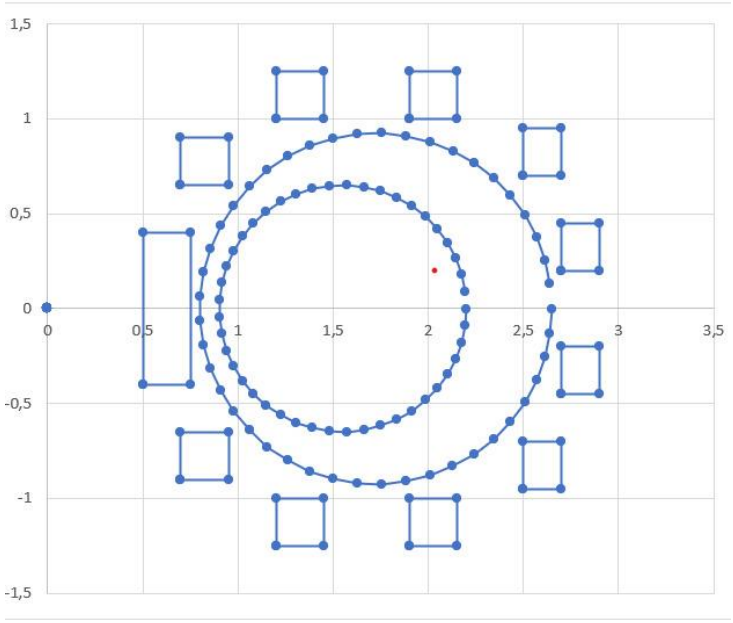

Figure 14: Spatial configuration of the poloidal field coils, the vacuum chamber and the C1 plasma contour.

The efficiency of the KBP matrix is defined by comparing the calculation of the flux on Cp to the iso flux theoretical value of 1 Weber. The values generated by the solution:

$\emptyset P = MPB * JB_m$, must be as close as possible to 1 Weber on the Np points of the contour Cp or C1.

We compared two main scenarios:

- Case Nb=11 and 11 constraints (exact flux on Nb points of contour C1), without smoothing the coil currents: Figure 15 and Figure 16.
- Case Nb=11 but 1 constraint (exact flux on interior point 1):
  - Without smoothing the coil currents: Figure 17 and Figure 18
  - With smoothing of the coil currents: Figure 19 and Figure 20

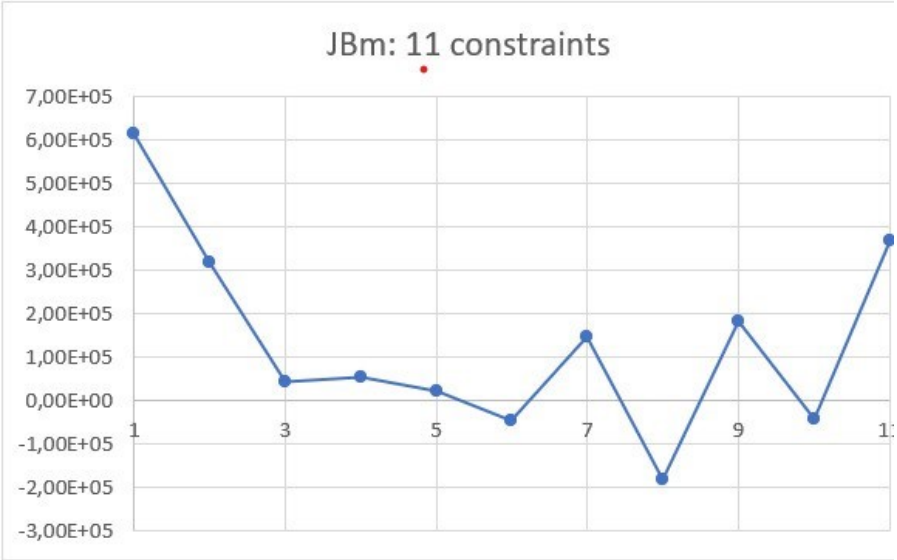

Figure 15: Magnetizing distribution according to the number of coils (case N=11 constraints)

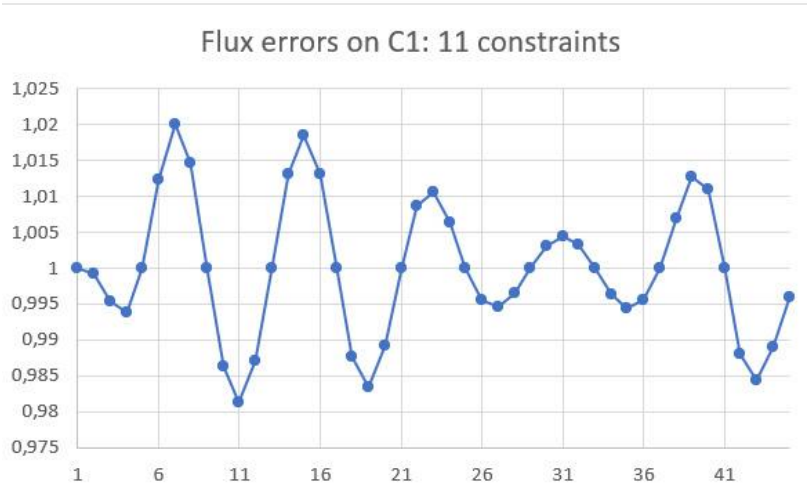

Figure 16: Distribution of the flux on C1 for the magnetizing distribution (case N=11 constraints)

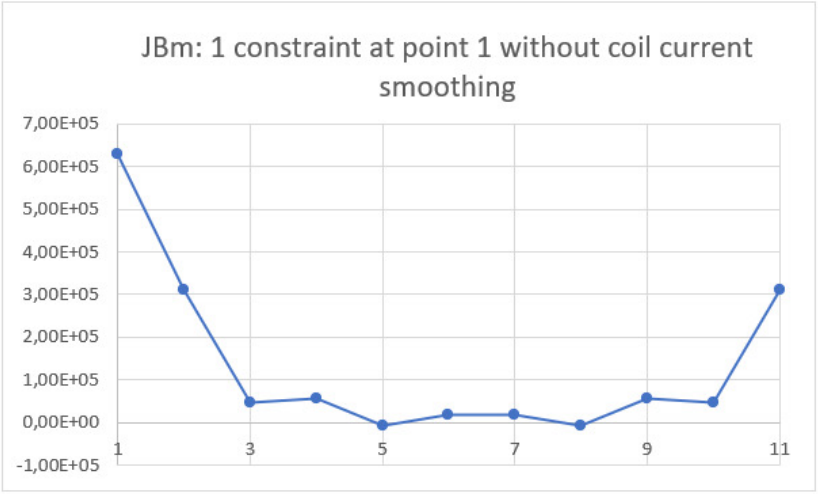

Figure 17: Magnetizing distribution according to the number of coils (case N=1 constraint at point 1) without smoothing the coil currents

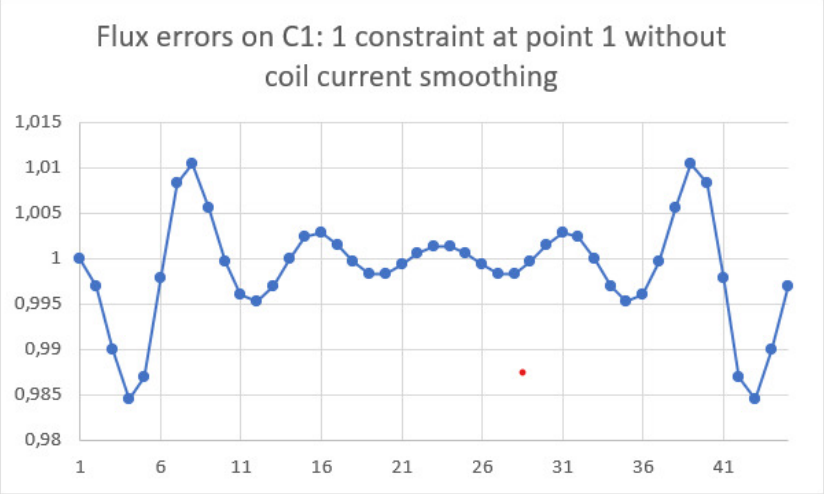

Figure 18: Distribution of the flux on C1 for the magnetizing distribution (case N=1 constraint) without smoothing the coil currents

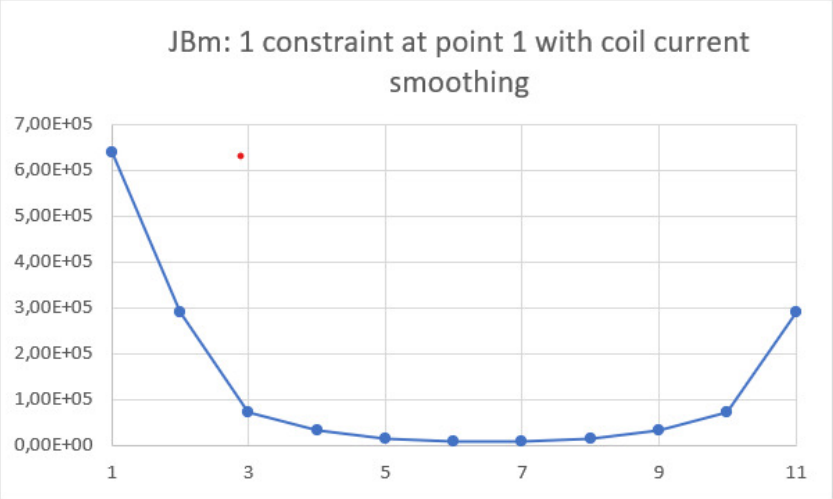

Figure 19: Magnetizing distribution according to the number of coils (case N=1 constraint at point 1) with additional smoothing of the coil currents

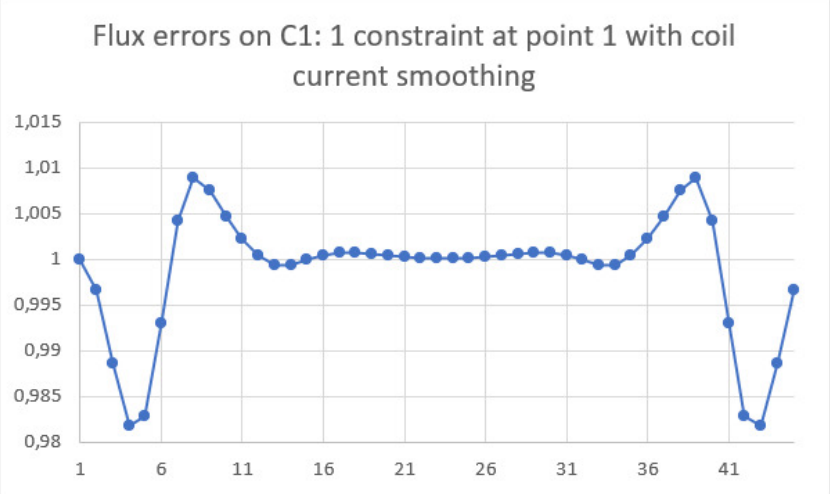

Figure 20: Distribution of the flux on C1 for the magnetizing distribution (case N=1 constraint) with additional smoothing of the coil currents

We therefore shown that using less constraints (One minimum constraint) leads to the improvement of the errors and the possibility to smooth the coil currents for a machine without iron core. In this example, we used 45 calculation points of the flux on C1 with the first point as exact flux. The results are better with less constraints compared to the case of Nb=11 constraints.

7.4. Approach to the solution of the plasma position control loop

7.4.1. Case of a very resistive vacuum chamber

Let us first assume that the vacuum chamber is very resistive (very short flux penetration time constant in the chamber) then the vacuum chamber can be neglected. The open loop equations, by ignoring the vacuum chamber as well as the plasma as an electrical conductor (§ 4.3) are:

Equation 15: Open loop equations

On the contour of the poloidal field coils Cb: $\emptyset B = MBB * JB$,

On the plasma contour Cp: $\emptyset P = MPB * JB$,

or versus the flux differences: $\emptyset P(i) = \emptyset P(1) + \Delta\emptyset P(i)$, for i=1 to Np

As mentioned in § 8, for a machine with a magnetic circuit, we will close the loop on the voltage of the generator(s) associated with the coil voltages (Vb), by the following expression, for example, with a proportional gain α:

a) $Vb = -\alpha * MBB * JB_e$, where:

JB_e, is the Jb solution satisfying: $JB_e = KBP * \Delta\emptyset P$, on Cp (C1) and α, a real positive number.

Then, the equation of the fluxes of the poloidal field coils is translated after derivation by:

b) $\frac{d\emptyset B}{dt} = Vb = MBB * \frac{dJB}{dt}$

By eliminating Vb between the two previous relations (a) and (b), we obtain:

$$MBB * \left[\frac{dJB}{dt} + \alpha * JB_e\right] = 0.$$

As MBB is an invertible matrix we necessarily deduce:

$$\frac{dJB}{dt} + \alpha * JB_e = 0 \quad \rightarrow \quad \frac{dJB}{dt} = -\alpha * JB_e$$

Thus, the flux equation on the contour CP is translated, after the elimination of JB and with the solution JBe by:

$$\frac{d\emptyset P}{dt} + \alpha * MPB * JB_e = 0$$

As the JBe solution satisfies: $MPB * JB_e = \Delta\emptyset P$, up to the error on Cp, and after replacement of the absolute fluxes on Cp by the differential fluxes and the common flux component: ∅P(1), the final closed loop equations become:

Equation 16: Closed-loop equations in the case of a highly resistive vacuum chamber

$$\frac{d\Delta\emptyset P}{dt} + \alpha * \Delta\emptyset P = 0$$

and

$$\frac{d\emptyset P(1)}{dt} = 0$$

The fluxes on the C1 contour therefore satisfy an always stable equation where the vector $\Delta\emptyset P$ tends towards zero with a common time constant: T=1/ α.

If we had closed the loop with an additional derivative gain: $-\beta * MBB * \frac{dJB_e}{dt}$, we would obtain the final equation which is also always stable:

$$(1+\beta) * \frac{d\Delta\emptyset P}{dt} + \alpha * \Delta\emptyset P = 0$$

With the common time constant:

$$T = \frac{1+\beta}{\alpha}$$

Thus, with a very resistive vacuum chamber, the control of the fluxes on Cp is always ensured and optimized: the differential fluxes on C1 converge towards 0, with the error: ε, according to the chosen Jb solution.

7.4.2. Influence of the vacuum chamber

In the case of low or even zero electrical resistance, the vacuum chamber is similar to a virtual hull. We showed, in § 2.2.4, that the magnetic configurations internal and external to the hull are, in this case, magnetically partitioned. In other words, no control of the interior conductors is possible using the exterior conductors and vice versa.

Between these two extreme situations where the resistance of the chamber goes from infinity to zero, there is a significant margin and we will estimate the phenomena encountered in the general case.

The vacuum chamber slows down the penetration of the magnetic field or flux, generated by the coils, towards the interior of the chamber where the plasma is located but this penetration time constant is not homogeneous along the contour of the chamber. In fact, there is not just one time constant but a set of N distinct time constants where N is the number of conductors modelling the vacuum chamber. The time constants specific to the vacuum chamber: τ, are determined from the time equation of the vacuum chamber:

$$MCC * \frac{dJC}{dt} + RCC * JC = 0$$

where: MCC is the mutual inductance matrix and RCC is the diagonal resistance matrix. They are expressed in terms of the N negative real solutions of the Laplace operator: p, which satisfy the equation:

$$Determinant[MCC * p + RCC] = 0, \text{ with: } \tau = -\frac{1}{p}.$$

This penetration time varies as the inverse of the resistance. It is all the greater as the resistance of the vacuum chamber is low. Finally, the greater this field penetration time, the longer the electrical voltage on the vacuum chamber must remain applied, going so far as to generate a distribution of currents, almost stationary on the chamber, which creates an undesirable flux at the level of the plasma, but which it is perhaps not necessary to compensate if its effect is considered acceptable with regard to the flux differences on the C1 contour.

Fortunately, the plasma control loop will be able to compensate for all these undesirable phenomena.

7.5. General solution of the plasma position control loop

7.5.1. Open loop equations

The electromagnetic equations, including the vacuum chamber, linking the fluxes and currents in the case of plasma displacement control, at Ip = constant, do not contain the plasma as an active conductor, according to § 4.3. In addition, the electrical resistances of the poloidal field coil circuit can be assumed to be null because they only affect the voltage of the associated generators:

$$Vg = Vb + Rb * JB,$$

where Vg is the voltage of the associated generator and Vb the real voltage of the coils.

The open loop equations are therefore defined by the following:

Equation 17: Open loop equations a, b, c and d

a) Flux on the Nb poloidal field coils:

$$\emptyset B = MBB * JB + MBC * JC$$

b) Flux on the vacuum chamber modelled by Nc conductors:

$$\emptyset C = MCB * JB + MCC * JC$$

$$\frac{d\emptyset C}{dt} + RCC * JC = 0$$

with: RCC = diagonal resistance matrix of the vacuum chamber.

d) Flux on Np (or N1) points of the C1 contour:

$$\emptyset P = MPB * JB + MPC * JC$$

where: $\emptyset P(i) = \emptyset P(1) + \Delta\emptyset P(i)$, for i=1 to Np.

At this stage, the objective would be to find the existing relationship between the fluxes on the C1 contour of the plasma and the fluxes of the poloidal field coils, after eliminating the intermediate variables, because we are going to close the loop on the voltages of the poloidal coils. It is the final relationship between $\emptyset P$ and $\emptyset B$, which would allow us to decide on the stability of the open or closed loop. In reality, with a passive shell like the vacuum chamber there are never any stability problems so the study of the stability of the loop, other than the conditions on the loop gains, is not necessary. Fortunately, because it is not possible to explicitly express the variable JC, current distribution on the vacuum chamber, to be able to eliminate it, unless the problem is solved numerically.

Thus, we will only eliminate the variable JB between these equations and define the unique equation satisfied by the vacuum chamber.

The variable: JB, is expressed from Equation 17-a:

$$JB = MBB^{-1} * \emptyset B - MBB^{-1} * MBC * JC$$

Then, we carry this expression into the other equations. The fluxes on the vacuum chamber becomes from Equation 17-b:

$$\emptyset C = MCB * MBB^{-1} * \emptyset B + [MCC - MCB * MBB^{-1} * MBC] * JC$$

which transforms by setting: $XCC = [MCC - MCB * MBB^{-1} * MBC]$, into:

$$\emptyset C = MCB * MBB^{-1} * \emptyset B + XCC * JC$$

Thus, from Equation 17-c, the final vacuum chamber equation becomes:

Equation 18: Equation of the vacuum chamber versus JC and $\emptyset B$

$$MCB * MBB^{-1} * \frac{d\emptyset B}{dt} + XCC * \frac{dJC}{dt} + RCC * JC = 0$$

Then, the flux on the plasma contour C1 becomes, from Equation 17-d:

$$\emptyset P = MPB * MBB^{-1} * \emptyset B + [MPC - MPB * MBB^{-1} * MBC] * JC$$

which transforms by setting: $XPC = [MPC - MPB * MBB^{-1} * MBC]$, into:

Equation 19: Equation of the fluxes on C1 versus JC and $\emptyset B$:

$$\emptyset P = MPB * MBB^{-1} * \emptyset B + XPC * JC \text{ and}$$

$$XPC = [MPC - MPB * MBB^{-1} * MBC]$$

7.5.2. Closed loop equations: closure relationships

We will close the loop at the level of the voltages of the poloidal field coils or generators associated with each coil, according to a general practice, comprising a proportional gain: α, a derived gain: β and an integral gain: γ, of the solution: JB_e. The gains: α, β and γ, are generally scalars but can be, in certain particular cases, matrix gains:

We will see in § 8 that this solution also applies to a machine with a magnetic circuit.

Equation 20: Relations of the loop closure

$$Vb = \frac{d\emptyset B}{dt} = -MBB * Jo$$

where:

$$Jo = \left[\alpha * JB_e + \beta * \frac{dJB_e}{dt} + \gamma * \int JB_e \,.\mathrm{dt}\right]$$

JB_e, is the previously calculated solution which satisfies on the C1 contour of the plasma (§ 7.2.3):

$$JB_e = KBP * \Delta\emptyset P$$

Either:

$$Jo = KBP * \left[\alpha * \Delta\emptyset P + \beta * \frac{d\Delta\emptyset P}{dt} + \gamma * \int \Delta\emptyset P \,.\, dt\right]$$

7.5.3. Closed loop: global equations

The vacuum chamber equation, from Equation 18, is expressed versus Jo, into:

Equation 21: Vacuum chamber equation versus Jo

$$XCC * \frac{dJC}{dt} + RCC * JC = MCB * Jo$$

The flux on C1, from Equation 19, is expressed after derivation versus time, into:

Equation 22: Fluxes on C1 equation versus Jo

$$\frac{d\emptyset P}{dt} + MPB * Jo = XPC * \frac{dJC}{dt}$$

We will show that, thanks to the specific KBP matrix, the vacuum chamber equation is practically independent of the loop gains; which means that even if we do not know the exact evolution of the JC currents, the maximum values of JC and its derivatives are bounded and only depend on the derivative of $\emptyset P$.

Let us eliminate the variable Jo between these two equations, from Equation 22 of the fluxes on C1, by multiplying on the left the two members of the equation by the KBP matrix whose following matrix product satisfies the identity matrix NbxNb:

$KBP * MPB \sim Ibb$, according to: Equation 12.

The expression of Jo becomes from Equation 22 of the flux expression on C1:

$$Jo \sim KBP * XPC * \frac{dJC}{dt} - KBP * \frac{d\emptyset P}{dt}$$

Then by replacing this expression in Equation 21 of the vacuum chamber, we then obtain the final approximate equation of the vacuum chamber:

Equation 23: Final approximate equation of the vacuum chamber

$$[XCC - MCB * KBP * XPC] * \frac{dJC}{dt} + RCC * JC + MCB * KBP * \frac{d\emptyset P}{dt} \sim 0$$

With: $XCC = [MCC - MCB * MBB^{-1} * MBC]$ and $XPC = [MPC - MPB * MBB^{-1} * MBC]$

The evolution of the current distribution: JC, is therefore practically independent on the loop gains, but only depends on the variable:

$$\frac{d\emptyset P}{dt}$$

The resulting time constants associated with the chamber current: JC, do not depend on the loop gains either. They are different and may be weaker than those evaluated with the vacuum chamber alone (§ 7.4.2). Thus, the peculiar matrix KBP allows to keep the evolution of the vacuum chamber current practically independent on the loop gains.

From Equation 23, we deduce the expression of the derivative of the JC distribution:

Equation 24: Derivative of the JC current distribution

$$\frac{dJC}{dt} = -ZCC^{-1} * \left[RCC * JC + MCB * KBP * \frac{d\emptyset P}{dt}\right]$$

with: $ZCC = [XCC - MCB * KBP * XPC]$

Either:

$$\frac{dJC}{dt} = -KCC * JC - KCP * \frac{d\emptyset P}{dt}$$

with: $KCC = ZCC^{-1} * RCC$ and $KCP = ZCC^{-1} * MCB * KBP$

We will now express the fluxes on the C1 contour of the plasma. Equation 22 of the fluxes on C1 becomes, as: $JB_e = KBP * \Delta\emptyset P$, and with the expanded expression of Jo of Equation 20:

Equation 25: General equation of the fluxes on C1 in closed loop

$$\alpha * \Delta\emptyset P + (1+\beta) * \frac{d\Delta\emptyset P}{dt} + \gamma * \int \Delta\emptyset P \,.\, \mathrm{dt} = XPC * \frac{dJC}{dt} - \frac{d\emptyset P(1)}{dt}$$

Assuming that the derivative term of JC of the second member of this equation is negligible or bounded, then we recognize the solution of § 7.4.1 (with $\gamma = 0$), with a highly resistive vacuum chamber. In general, this term cannot be neglected. Then, we will express the derivative of JC from Equation 24, of the vacuum chamber and report it in the previous Equation 25, as follow:

Equation 26: Final equation of fluxes on C1 in closed loop

$$\gamma * \int \Delta\emptyset P \,.\, dt + \alpha * \Delta\emptyset P + [(1+\beta) * Ipp + XPC * KCP] * \frac{d\Delta\emptyset P}{dt} = -[1 + XPC * KCP * Vp] * \frac{d\emptyset P(1)}{dt} - XPC * KCC * JC$$

Where, Ipp is the identity matrix NpxNp and Vp, the unit column vector Npx1.

We can now see that the second member of the equation no longer contains the derivative of JC but only JC, which changes little in amplitude, especially when the loop time constants are small: between 10 ms and 100 ms. At the convergence of the first member of this equation, the static error at convergence is always low. It decreases as the inverse of the proportional or integral gain.

We will now deduce the two main solutions based on the loop gains.

7.5.4. The main solution with proportional and derivative gains

The integral gain γ is zero, then the new closed-loop equation is expressed from Equation 26 by:

$$\alpha * \Delta\emptyset P + [(1+\beta) * Ipp + XPC * KCP] * \frac{d\Delta\emptyset P}{dt} = -[1 + XPC * KCP * Vp] * \frac{d\emptyset P(1)}{dt} - XPC * KCC * JC$$

This time we note that the term of the second member in: JC, evolves little in amplitude compared to its derivative. The first member of this equation converges for: $\alpha > \beta$ and $\alpha \gg 1$, but the convergence time constants of the fluxes on the points of the contour C1 are very different with a scalar proportional gain and evolve in average value around:

$$T \sim \left(\frac{1+\beta}{\alpha}\right)$$

On the other hand, by replacing the proportional scalar gain: α, by the following proportional matrix gain, coefficient matrix of the derivative term of $\Delta\emptyset P$:

$$\alpha * GA = \alpha * [(1+\beta) * IPP + XPC * KCP],$$

the convergence time constant is, this time, unique on all points of the fixed C1 contour and equal to: $T = \frac{1}{\alpha}$, with a final equation defined by:

Equation 27: Solution with matrix proportional gain and scalar derivative gain

$$[(1+\beta) * Ipp + XPC * KCP] * \left[\Delta\emptyset P + \left(\frac{1}{\alpha}\right) * \frac{d\Delta\emptyset P}{dt}\right] = -\left(\frac{1}{\alpha}\right) * [1 + XPC * KCP * Vp] * \frac{d\emptyset P(1)}{dt} - \left(\frac{1}{\alpha}\right) * XPC * KCC * JC$$

Or again, as the matrix: GA, of proportional gain is invertible:

Equation 28: Final closed loop equation with matrix proportional gain and scalar derivative gain

$$\Delta\emptyset P + \frac{1}{\alpha} * \frac{d\Delta\emptyset P}{dt} = -\frac{1}{\alpha} * [(1+\beta) * Ipp + XPC * KCP]^{-1} * \left[(1 + XPC * KCP * Vp) * \frac{d\emptyset P(1)}{dt} + XPC * KCC * JC\right]$$

The $\Delta\emptyset P$ converge to a value close to zero with a common time constant: $T = \frac{1}{\alpha}$, and with a static error at convergence that is all the smaller as: α and β are large.

The value of α, must evolve between 10 and 100, for a convergence time constant varying from 10 ms to 100 ms. The value of β, evolves from 0 to approximately: 10, or even more.

This solution with proportional matrix gain and scalar derivative gain, is simple and optimal, but it requires the prior calculation of the matrices: XPC and KCP, defined in Equation 23 and Equation 24.

Equation 29: Expression of the matrices XPC et KCP

The matrix: XPC, is expressed as a function of the basic matrices, according to Equation 19 by:

$$XPC = [MPC - MPB * MBB^{-1} * MBC]$$

The matrix: KCP, is expressed from Equation 18 and Equation 24, by:

$$KCP = [MCC - MCB * KBP * MPC]^{-1} * MCB * KBP$$

In summary, this optimal solution requires a scalar derivative gain: β and a matrix proportional gain: $\alpha * GA$, defined by:

$$\alpha * GA = \alpha * [(1+\beta) * IPP + XPC * KCP]$$

7.5.5. The solution with integral gain

The equation with integral gain γ, is obtained after derivation of Equation 26:

$$\gamma * \Delta\emptyset P + \alpha * \frac{d\Delta\emptyset P}{dt} + [(1+\beta) * Ipp + XPC * KCP] * \frac{d^2\Delta\emptyset P}{dt^2} = -[1 + XPC * KCP * Vp] * \frac{d^2\emptyset P(1)}{dt^2} - XPC * KCC * \frac{dJC}{dt}$$

Then, by replacing the derivative of JC by its value expressed in Equation 24:

$$\gamma * \Delta\emptyset P + [\alpha * Ipp - XPC * KCC * KCP] * \frac{d\Delta\emptyset P}{dt} +$$

$$[(1+\beta) * IPP + XPC * KCP] * \frac{d^2\Delta\emptyset P}{dt^2}$$

$$= -[1 + XCP * KCP * Vp] * \frac{d^2\emptyset P(1)}{dt^2} + XPC * KCC * KCP * Vp * \frac{d\emptyset P(1)}{dt} + XPC * KCC * KCC * JC$$

In this system of differential equations of order 2, it is necessary to use the three scalar gains simultaneously: α, β and γ, with, for each, values greater than 10; high gains make it possible to make the diagonal of each matrix, preponderant compared to the other terms of this matrix. In order to ensure the stability of the system with, preferably, real time constants, the gains must verify the inequality:

$$\alpha^2 - 4 * (1+\beta) * \gamma \geq 0$$

In addition, the two real time constants must be comprised between 10 ms and 100 ms.

Convergence is ensured but the solution with integral gain is more complex and does not provide anything more than the previous general solution with proportional and derivative gains. Indeed, the static error at convergence remains with the term in JC and the convergence time constants of the fluxes on C1 are different. In principle, the presence of an integral gain cancels the static error but given the impossibility of explicitly expressing JC and its derivatives in order to eliminate them, the integral gain can never cancel the convergence error.

7.6. Possible instabilities of the plasma position control loop

We have just seen that the plasma position control loop is always stable provided that the relationships between the loop gains are respected, but with high gains certain conditions must be respected, such as for example the progressive switching of the plasma control loop. Otherwise, the coil voltages generated by the loop can saturate the generators and create oscillatory phenomena with a risk of loss of control and therefore disruption of the plasma.

7.7. Conclusion on the plasma position control loop

The control loop of the plasma displacements must be closed at the level of the voltages of the poloidal field coils, in general, using gains: proportional, derivative, and/or integral, scalar or matrix of the variable: $\Delta\emptyset P$, according to Equation 20.

This control loop applies, indifferently, to a machine with or without a magnetic circuit (§ 8). The gains are generally scalars with the exception of the optimal solution of § 7.5.4, comprising a proportional matrix gain and a scalar derivative gain. This optimal solution requires the calculation of the matrix: GA, associated with the proportional gain: α but the convergence time constants of all the points of the contour C1 are identical: $T = \frac{1}{\alpha}$. The static error at convergence decreases with increasing gains: α, varying from 10 to 100 and β varying from 0 to 10, for a convergence time constant comprised between 10 ms and 100 ms.

The use of the particular KBP matrix, to close the control loop, makes the evolution of the JC current distribution of the vacuum chamber independent of the loop gains. The vacuum chamber equation, thus defined, allows the correct evaluation of the solutions of the plasma position loop, totally decoupled from the vacuum chamber.

Finally, the increase in the resistivity of the metal constituting the vacuum chamber promotes the performance of the loop by reducing the convergence error at constant gains.

7.8. Plasma current amplitude control

7.8.1. Simplified control

The control of the plasma current, after the plasma initiation period, can be achieved by simply controlling the central coil voltage. As the external field necessary for plasma equilibrium depends on the internal distribution of the plasma current, any modification of the plasma current will generate flux deviations on C1 which are completely controlled by the plasma

position loop. It is simply necessary to control the plasma current with a time constant greater than those linked to the plasma movements. This current control loop is therefore slower in order to maintain plasma equilibrium when Ip varies.

7.8.2. Plasma current control using the magnetizing distribution

If we want the coil currents, for a machine without a magnetic circuit, to always be shaped by the previous solution: JBe, it is recommended to control the current Ip using the magnetizing component: JBm, of the JB solution.

It is not complicated to implement a current control loop Ip using an exponential slope limiter filter where the error: $\varepsilon = Ip - Io$, (Io = current reference) is first applied to the filter input. The output: S, of the filter, amplified by the gain: g, is then reinjected into the loop:

Equation 30: Plasma current control by using the magnetizing component

$$\frac{d\emptyset B}{dt} = Vb = -MBB * KBP * Vp * g * S$$

where: Vp dimension is: Npx1, with: $Vp(i) = 1$ for i=1 to Np

8. Machine with magnetic circuit

8.1. Modelling the presence of iron placed in a magnetic field

8.1.1. Relationship between induction and magnetic field

The relationship between the magnetic induction: $\vec{B}$, and the magnetic field: $\vec{H}$, depends on the environment or material in which the magnetic configuration is located, according to the relation:

Equation 31: Relationship between magnetic induction and magnetic field

$$\vec{B} = \mu_r * \mu_o * \vec{H},$$

Where: $\mu_o = 4.\pi.10^{-7}\frac{H}{m}$, in Henry per meter, universal constant, is the magnetic permeability in vacuum or in air and μ_r, the relative magnetic permeability which depends on the environment or material. For the iron, the magnetic permeability value varies from several hundred to 5000.

Furthermore, in an environment with no internal real current distribution, the field verifies:

$$\overrightarrow{Rot}(\vec{H}) = \vec{0}$$

8.1.2. Modelling the effect of μ_r in air or vacuum

Consider an environment whose relative permeability: μ_r, depends on space (x, y, z) then, is there a model in air or vacuum which allows us to transpose the electromagnetic equations of any environment, into vacuum or air?

If this is the case, then, the virtual field: $\overrightarrow{H_{air}} = \mu_r * \vec{H}$, in air or vacuum satisfies:

$$\vec{B} = \mu_o * \overrightarrow{H_{air}}.$$

Let us then calculate the rotational of: $\overrightarrow{H_{air}}$; we easily demonstrate that:

Equation 32

$$\overrightarrow{Rot}(\mu_r * \vec{H}) = \mu_r * \overrightarrow{Rot}(\vec{H}) + \overrightarrow{Grad}(\mu_r) \times \vec{H},$$

where: ×, represents the cross product of the two vectors.

We deduce, as: $\overrightarrow{Rot}(\vec{H}) = \vec{0}$, in the environment of iron free from real current distribution, that:

Equation 33: Expression, in air, of the virtual current density located in the volume occupied by the material

$$\overrightarrow{Rot}(\overrightarrow{H_{air}}) = \overrightarrow{Grad}(\mu_r) \times \vec{H} = \vec{J}$$

In conclusion, the magnetic configuration in an environment of a variable relative permeability: μ_r, can be replaced by a magnetic configuration in a vacuum or air, thanks to the distribution of a virtual volume current density: $\vec{J}$, which replaces the initial environment at all points of its volume.

8.2. Modelling in the air of a machine with a magnetic core

We showed in the previous section that the iron of the magnetic circuit can be replaced by a volume distribution of current, in the air: $\vec{J}$, located in the volume of the iron. On the other hand, we showed in § 3.2, that this external distribution can be replaced by a virtual current distribution: JF, located on a contour, placed inside the magnetic circuit, with respect to the magnetic configuration inside the contour Cf, which contains all of the machine's conductors, according to Figure 21, below.

This current distribution: JF, varies in a non-linear manner depending on the real current distribution: JBr, of the coils and the characteristics of the iron. Knowledge of the exact evolution of this virtual distribution is of little importance for our demonstration. Let MBF be the matrix of mutual inductances, in the air, between the JF distribution of the iron contour Cf and the poloidal field coils (Cb contour). The flux emitted by the iron in the poloidal field coils is expressed by:

$$\emptyset Bf = MBF * JF$$

The contour Cb of the coils is interposed between the contour of the iron and that of the vacuum chamber containing the plasma. As a result, it plays the role of an electro-magnetic screen or “holed” hull and assuming that the coils are well distributed and in sufficient number, the flux emitted by the iron inside the machine can be completely screened by the distribution: $-JBf$, of the coils such as:

$$MBB * JBf = MBF * JF \rightarrow JBf = MBB^{-1} * MBF * JF$$

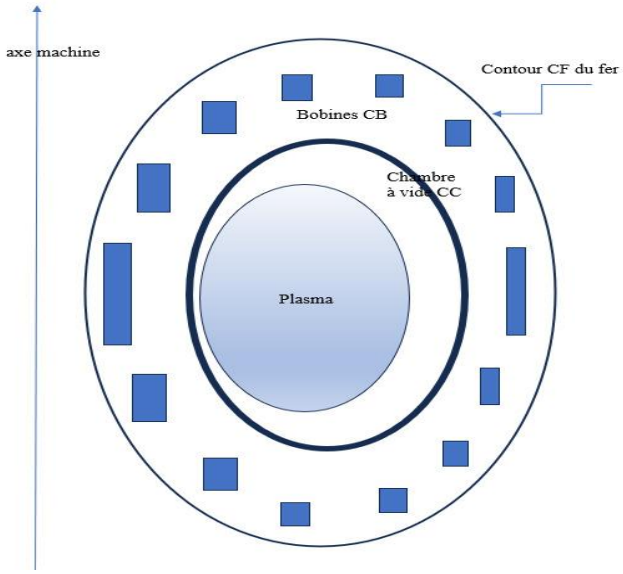

Figure 21

Under these ideal conditions, the leakage flux emitted by the iron at the level of the plasma is null and the magnetic circuit, including the contour Cf supporting the: JF, current distribution, can be simply replaced by a virtual current distribution JBt, located in the poloidal field coils, located this time, in the air and equal to:

$JBt = JBr + JBf$, with: JBr =real currents of the coils.

In conclusion, assuming a perfect screening of the flux emitted by the iron by the poloidal field coils, the influence of the magnetic circuit can be modelled by a virtual current JBf, located in the poloidal field coils placed in the air. This means

that the JBe solution in the air does indeed exist under these conditions and is calculated according to § 7.2.3, with only the poloidal field coils, in the air, as if the magnetic core did not exist.

8.3. Main case with incomplete screening of the iron effect

In the general case, the flux emitted by the iron is not completely screened by the poloidal field coils, the number of which is too small. When the iron is not saturated, the magnetizing flux circulates mainly in the magnetic circuit and does not reach the plasma, but when the central core saturates, part of the magnetizing flux closes in the air at the central coil and reaches the plasma contour.

This leakage flux in the air evolves relatively slowly compared to the speed of the plasma position loop and can therefore be compensated in real time.

Thus, in the general case, we will calculate the KBP matrix as for a machine without a magnetic circuit. In this case, the leakage flux of the unscreened iron flux must be considered as a disturbance in the same way as the chamber currents and will be compensated by the plasma position control loop.

8.4. Conclusion on the effect of a magnetic core

Thus, the magnetic circuit of the machine will be completely ignored for the calculation of the plasma position control loop. The KBP matrix will be calculated in air (§ 7.2.3) and the loop will be closed according to Equation 20, established for a machine without magnetic circuit.

9. Machine with magnetic divertor

In this chapter, we assume that real-time plasma data are not necessary for plasma control and zero-field points. Simulations, based on plasma current profiles, are performed only to demonstrate their physical feasibility in advance and to optimize machine parameters.

9.1. Introduction

A machine with a magnetic divertor is characterized by the presence of one or two additional coils, located in the vacuum chamber near the plasma. The objective is to create one or two points (top and/or bottom) of zero-magnetic field in order to be able to collect the particles located on the external surface of the plasma including helium, plasma “ashes” resulting from partial fusion reactions as well as certain metal waste torn from the wall of the vacuum chamber by the plasma (Figure 22).

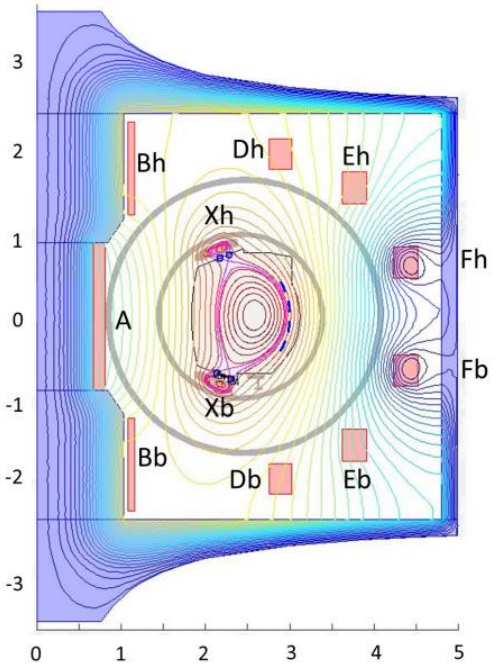

Figure 22: Vertical cross section of the TORE SUPRA-WEST version machine with double X point from the CEA of Cadarache (France)

9.2. Influence of the "divertor" coil currents on the plasma equilibrium

Let us assume that we know the plasma boundary Cp (or C1), then, for a machine in air, therefore without a magnetic circuit, the flux equation on the plasma contour translates, ignoring the plasma as a conductor (§ 4.3), by:

$$\emptyset P = MPB * JB + MPD * JD + MPC * JC, \text{ on the plasma contour: Cp (or C1).}$$

This equation includes an additional term: $MPD * JD$, compared to a conventional machine without magnetic divertor. The JD ampere-turns are controlled to establish one or two zero-field points. The divertor coils cannot therefore be used for plasma position control. On the contrary, the JD currents disturb the fluxes on the plasma contour and therefore the plasma equilibrium. It is clear that only the poloidal field coils will control the plasma equilibrium and that these flux deviations generated by the divertor coil currents on the plasma contour must be cancelled by the poloidal field coils.

The general solution will consist in considering the JD currents and their variation as an external disturbance to the plasma position control loop, in the same way as the vacuum chamber currents or the iron leakage flux. The vertical instability of the plasma in its elongated form, generated by the zero-field points, is mainly due to the presence of the JD currents and their variation. As the JD currents are known in real time, it is strongly recommended to integrate a preprogramming of the fluxes of the poloidal field coils, for a machine in air or with a magnetic circuit, which oppose the flux deviations generated by the "divertor" coils on the fixed envelope of the plasma boundaries (§ 9.3.2), by ignoring the vacuum chamber, according to the equation:

Equation 34: Cancellation of flux deviations generated by *JD* current distribution, ignoring the vacuum chamber

$$d\emptyset B = -MBB * KBP * d(\Delta\psi),$$

where: $\Delta\psi$, are the differential fluxes generated by the JD currents, calculated from the flux matrix on the controlled contour: $\psi = MPD * JD$ and the KBP matrix, calculated according to § 7.2, on the contour of the plasma boundary envelope. Indeed, making the fixed contour Ce iso flux in the presence of only the currents: JD, allows to cancel the distribution of the magnetic field generated by the currents: JD, inside the envelope Ce, independently of the size or position of the plasma, located inside the envelope. As the reference contour of flux control is a fixed contour: the envelope of the plasma boundaries, the previous equation translates to:

Equation 35: Pre-programming voltage for compensating for flux deviations generated by *JD* currents

$$VB_{prog} = \frac{d\emptyset B}{dt} = -KBD * \frac{dJD}{dt}$$

Where, the matrix KBD is a constant matrix of dimension: NbxNd.

In general, the installation of the currents JD, must be carried out just after the plasma initiation phase, during the growth phase of the plasma current from the moment when the generators associated with the poloidal field coils are in service or later, at the beginning of the plateau phase of the plasma current.

During the growth of the divertor currents: JD, the preprograming voltage (Equation 35) must not exceed 20% of the maximum voltage of each generator in order to allow the control of the plasma current and that of the plasma equilibrium. The limitation of the derivative of JD must be able to allow the rapid growth of the « divertor » currents, to obtain the zero-field points; also, we suggest limiting the derivative of the current: JD, using an external inductance, if necessary, connected in series with each divertor coil. We will see in § 9.5.2, the advantages of the presence of this inductance.

This preprograming voltage of open loop compensation of the effect of the JD currents at the level of the poloidal field coils, even ignoring the vacuum chamber, allows to greatly reduce the stress on the plasma position control loop. It

therefore allows, apart from the influence of the currents induced in the vacuum chamber, to make the control of the zero-field points and that of the plasma practically independent.

The poloidal field coils will always control the position of the plasma as for a machine without a divertor. We will see how this control can be achieved in the following §.

9.3. Control of the plasma equilibrium

9.3.1. Foreplay

We treated, in the previous section 7, the case of a plasma with a constrained boundary on the fixed contour C1 and showed that the flux deviations on the contour C1 are cancelled by the plasma position control loop by reinjecting them at the coil voltage level using a particular matrix (Equation 20). This rule remains valid for a machine with or without a magnetic circuit. In this case, it involves controlling the flux on the fixed contour: C1, desired iso flux, using poloidal field coils. Furthermore, we showed in § 7.5.4 that the plasma convergence time constant (in seconds) on its contour is equal to the inverse of the scalar proportional gain in the case of a control loop with proportional matrix gain and scalar derivative gain.

In the case of a machine with a divertor, the plasma boundary as well as the zero-field point evolve in space, depending on the internal profile of the plasma for a fixed waste extraction zone in the vacuum chamber. We will show that despite the changing shape of the plasma boundary the problem of plasma equilibrium is also solved by controlling the flux deviations, but on a variable contour unlike a plasma with a constrained boundary.

9.3.2. Principle of plasma boundary identification

The different cases of plasma equilibrium with magnetic "divertor," calculated according to the different plasma current profiles and obtained by solving the "Grad-Shafranov" equations show a slight spatial variation of the plasma boundaries. We will therefore consider the outer envelope curve of all these elliptical-shaped boundaries, thus calculated. This curve, noted: Ce, the envelope of the plasma boundaries contains all the plasma sections studied according to the internal distribution of the plasma current.

We will now define the presumed plasma boundary on which the flux deviations will be calculated as in the case of a machine with constrained boundary.

We know how to calculate in real time the fluxes $\emptyset(i)$ and the tangent fields: $Bt(i)$, on a large number of points: M(i), of this fixed envelope curve, thanks to the current distribution: Jp, located on a fixed contour positioned inside all the calculated plasma boundaries and which satisfies the magnetic measurements. As the plasma boundary is located close to the envelope, we can affirm that a limited development of the flux on the envelope, according to the normal to the envelope, to the first order, is sufficient to estimate the fluxes up to the presumed plasma boundary according to the equation:

Equation 36: Limited development of flux from the envelope to the plasma

$$\emptyset_o = \emptyset(i) + 2 * \pi * r(i) * Bt(i) * d(i), \text{ where:}$$

- $\emptyset_0$, the value of the uniform flux on the plasma boundary,
- $\emptyset(i)$, the flux at each point M(i) of the envelope for i=1 to Np > Nb,
- $r(i)$, radial distance from point M(i) to the machine axis,
- $Bt(i)$, the tangential field at point M(i) of the envelope,
- $d(i)$, the distance according to the normal at point i, from M(i) to the plasma boundary.

We will note: P(i), the points calculated, according to the previous equation, distant from d(i) according to the normal to the envelope at the points M(i), with:

Equation 37: Expression of d(i)

$$d(i) = \frac{(\emptyset_0 - \emptyset(i))}{K(i)}$$

and $K(i) = 2 * \pi * r(i) * Bt(i)$

Finally, we will define: $\psi(i)$, the fluxes calculated at points P(i), which correspond to the fluxes on the presumed boundary of the plasma, located inside the envelope.

The existence of the solution of the exact plasma contour requires knowledge of the flux: $\emptyset_0$, on the plasma boundary. In other words, it is necessary to define, at least, a fixed reference point on the envelope, common to all calculated plasma boundaries, on which the flux on the supposed plasma boundary is calculated.

We will first define the fixed reference point where all plasma boundaries pass: for example, the point M(1), located on the envelope: Ce. The choice of this reference point is not trivial; it is the point, common to all free plasma boundaries. There is therefore no constraint on the plasma boundary, with this definition, whose boundary remains free; the value of the distance: d(1), is therefore zero since M(1) is located on the envelope. The exact plasma boundary is determined when it passes through point M(1).

In the main case, this point, common to all the free plasma boundaries, does not exist, and it will be necessary to choose a fixed point on which the plasma boundary will be forced and which is compatible with the establishment of a free zero-field point (§ 9.5). The plasma boundaries envelope shall be assessed with all constraints, including the reference point location.

The value of the flux: $\emptyset_0$, on the plasma boundary will therefore be that calculated at the fixed-point M(1) where the boundary is supposed to pass:

$\psi(1) = \emptyset_0$, at point M(1) of the envelope

Thus, if the plasma boundary actually passes through point M(1), where the flux is calculated, then the presumed plasma boundary is exact and completely determined; the fluxes: $\psi(i)$, calculated at points P(i) are all equal to $\emptyset_0$, to the nearest second order.

9.3.3. Principle of plasma position control

Let us imagine that the plasma has moved away from its previous equilibrium position, then the presumed plasma boundary calculated with a flux at point M(1) equal to ψ(1), is no longer iso flux but allows the calculation of the new values of d(i) defining the new presumed plasma boundary passing through point M(1) where: d(1)=0.

The calculation of the fluxes $\psi(i)$ at the new points P(i) allows the evaluation of the flux deviations with respect to point M(1). Assuming that it is possible to cancel these flux deviations, then using the same law for calculating the presumed boundary will force the points P(i) associated with the term d(i) to converge towards the exact boundary of the plasma with, at equilibrium: $\psi(1) = \emptyset_0$, at point M(1).

We will see in the following section, how to express the flux deviations.

9.3.4. Principle of calculating the flux deviations

We will now determine the flux deviations on the presumed plasma contour in the case where the plasma moves due to a magnetic disturbance internal or external to the plasma.

We will distinguish two cases, depending on the sign of d(i):

- Case $d(i) > 0$, where the presumed plasma boundary remains inside the envelope:

If the plasma boundary moves away from point M(1) then the flux calculated at point M(1): $\psi(1)$, becomes different than $\emptyset_0$, the flux value on the plasma boundary. We will calculate the new values of d(i) with the value of $\psi(1)$, as the flux reference value on the presumed plasma boundary which is therefore no longer iso flux and then we will determine the flux deviations on the presumed plasma contour at the new points P(i):

$$\Delta\psi(i) = \psi(i) - \psi(1), \text{ not null for: } i = 2 \; to \; Np.$$

This calculation is similar to that of a plasma with a constrained boundary on a fixed contour. In the present case, the presumed plasma contour is not fixed but evolves over time inside the envelope.

- Case $d(i) \leq 0$, where the plasma boundary overlaps the envelope at some points:

In this specific case, some consecutive values of d(i) become negative. This simply means that the associated points P(i) are located outside the envelope. The flux deviations at points P(i) where d(i) is negative, will then be calculated at points M(i) on the envelope by:

$$\Delta\psi(i) = \emptyset(i) - \psi(1), \text{ at points M(i) where: } d(i) \leq 0.$$

Indeed, in this case the envelope is the physical limit that the plasma must not cross as in the case of a fixed boundary.

The flux deviations on the other points P(i) remaining inside the envelope will be calculated as in the case of positive d(i).

In summary, the flux deviations on the presumed plasma boundary will be calculated as follows, depending on the sign of d(i), for i=2 to Np and with: $\emptyset_0 = \psi(1)$, in Equation 37:

- If $d(i) > 0$, then: $\Delta\psi(i) = \psi(i) - \psi(1)$, else:
- If $d(i) \leq 0$, then: $\Delta\psi(i) = \emptyset(i) - \psi(1)$.

9.3.5. Controlling the displacements of a plasma with a free boundary

We defined in the previous section how to calculate the flux deviations on the presumed plasma contour.

These flux deviations will then be reinjected into the plasma position control loop at the level of the poloidal coil voltages using the KBP matrix, calculated, in this case, on the fixed contour of the envelope: Ce, with the constraint of an exact flux at point M(1) and using only the poloidal field coils, according to § 7.2. The plasma position control loop will be closed as described in § 7.5.4, according to the optimum solution with proportional matrix gain and scalar derivative gain.

The plasma control loop allows the plasma boundary to be forced to pass through point M(1) and to keep the plasma inside the envelope.

9.4. Control of the plasma current

The plasma current control would be achieved from subsection 7.8.

9.5. Control of the zero-field point and of the associated separatrix

9.5.1. Foreplay

The zero-magnetic field point(s) are generated using one or two additional coils (Cd contour) located in the vacuum chamber and positioned near the plasma in the upper and/or lower part. For a given plasma current Ip, there is a current value JD, in the same direction as that of the plasma, which allows the generation of one or two zero-field points. As the plasma adapts and deforms with the magnetic field, the solution is difficult to put into an equation without coupling with a calculation code. It is necessary to generate a zero-field point but also to simultaneously control the separatrix passing through this zero-field point by ensuring that the latter enters the impurity absorption cavity, at two fixed points located on the divertor coil, as illustrated in Figure 23, below.

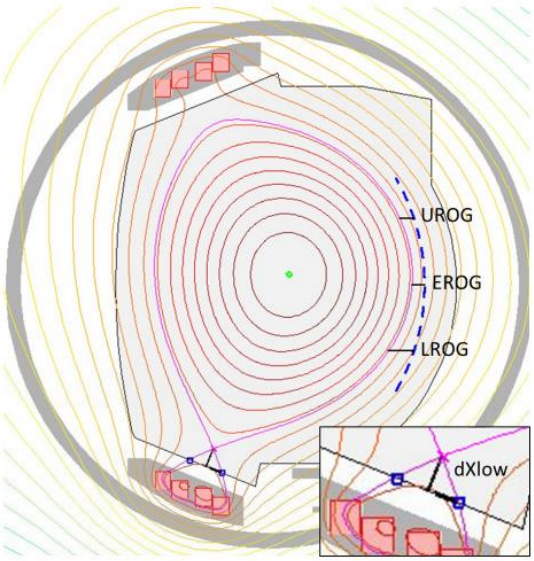

Figure 23: Case of operation with a single low X point of the Tokamak TORE SUPRA WEST version.

In the case of a constrained zero-field point: either fixed or positioned on a trajectory defined in advance, it will be necessary to couple plasma data in real time and to deform the plasma boundary to ensure convergence towards the desired zero-field point. This procedure is not flexible and requires coupling plasma equilibrium calculation data.

In the case of a free zero-field point, the convergence solution towards the zero-field point occurs naturally and does not require, in general, deformation of the plasma boundary. It is this latter, more flexible and simpler solution that we will develop.

9.5.2. Principle of control of a free zero-field point

The general control of the zero-field points requires that the separatrix of the zero-field point(s) always pass through two fixed points (C and D), located on the "divertor" coil, for all profiles of the plasma, as shown in the previous figure and schematized in Figure 24, for each of the two "divertors". This constraint allows the correct evacuation of the waste generated by the plasma in the cavities of the "divertor."

The principle of controlling the existence of one or two zero-field points is based on the equality of the fluxes at the fixed points C and D: $\emptyset_C = \emptyset_D$, of each coil since the separatrix passing through these two points is iso flux when the zero-field point is reached. Indeed, with the only distribution: JD, incoming:

$$\Delta\emptyset = \emptyset_C(JD) - \emptyset_D(JD) < 0$$

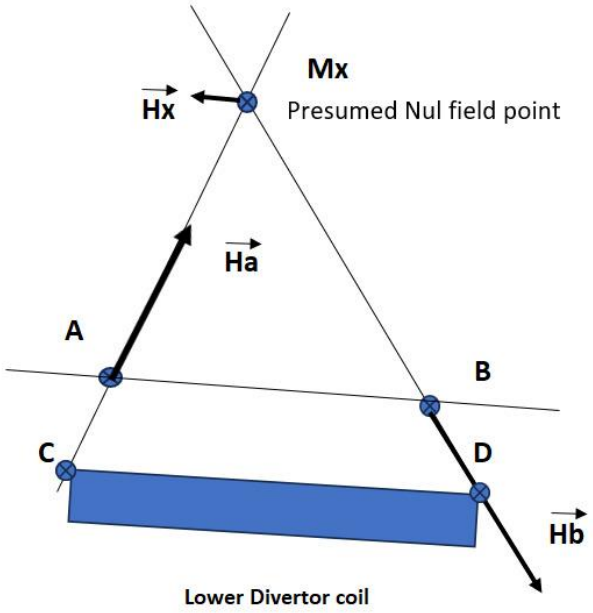

Figure 24: Zero-field point Mx with separatrix passing through two fixed points C and D, for a plasma current and a divertor current of same sign

It is the point D whose distance from the axis of the machine is the greatest which sees the highest flux. Thus, with only the plasma current, entering, $\Delta\emptyset$ is positive.

We saw in § 9.2 that the derivative of the currents: JD, must be limited in maximum value during the growth of the currents: JD, in order to allow the control of the position of the plasma and that of the plasma current with only 80% of the maximum voltage of the generators associated with the poloidal field coils. It is suggested to install an external inductance connected in series with each "divertor" coil. The value of this inductance must be as large as possible and limited to a value allowing the growth of the current: JD, with a derivative equal to 1.2 to 1.5 times the maximum value required for the installation of the zero-field point. The presence of this inductance makes it possible to significantly reduce the electromagnetic disturbances generated by the currents: JD and their variation. There is no more high-frequency chopping of the generator voltage.

Moreover, thanks to this smoothing inductance, the currents of the divertor coils can be simply voltage controlled using a scalar proportional gain: G, i.e. a generator voltage: Vd, defined by:

$$Vd = G * (\emptyset_C - \emptyset_D), \text{ with: } G > 10.$$

This simple control of the free zero-field point, associated with each divertor coil, requires the installation of two absolute flux loops, positioned at points C and D of each coil. This simplified control does not allow us to determine the spatial position of the zero-field point(s) but we only know that they exist.

We will see in the next section, the possibilities offered to assess in real time the spatial position of the zero-field points.

9.5.3. Principle of calculating the position of a free zero-field point

The calculation of the position of zero-field point is based on the assumption that the separatrix portions between the zero-field point Mx and the fixed points (C and D), located on the divertor coils, can be assimilated to portions of straight lines as illustrated in Figure 24.

Assuming that it is possible to install external field measurements at points C and D (vertical and radial fields), then the slopes of the lines Mx-C and Mx-D are directly determined by the components of the fields measured at points C and D, to the nearest sign. The position of the zero-field point can thus be calculated in real time at the point of intersection of the lines: Mx-C and Mx-D, when the condition: $\emptyset_C - \emptyset_D = 0$, is reached.

Without external field measurement, it will be necessary to use the Jp solution to calculate the fields at points A and B, positioned inside the contour of the magnetic measurements and located respectively on the lines Mx-C and Mx-D. Points C and D being fixed, points A and B are therefore mobile and it is necessary to define a criterion that allows to determine the position of points A and B in real time. Finally, we will note that when the zero-field point is reached, the fluxes at points A, B, C and D are equal, that is when: $\emptyset_A = \emptyset_B$ or $\emptyset_C = \emptyset_D$.

It is still necessary to know how points A and B, mobile, are defined in real time; this is what we will see in the next section.

9.5.4. Positioning criteria for points A and B

Since points C and D are fixed, we must first define a criterion that allows us to determine the position of points A and B such that the fields at points A and B are always aligned according to the respective directions of the slopes of lines A-C and B-D, defined by the components of the fields: $\overrightarrow{Ha}$ and $\overrightarrow{Hb}$, at points A and B.

Let us define an initial position of the moving points A and B such that lines C-A and D-B converge. Let us then calculate the magnetic fields at points A and B. Then, the two calculated fields: $\overrightarrow{Ha}$ and $\overrightarrow{Hb}$, are generally not aligned with the slopes of the two respective lines but define the slopes of the lines for the next iteration. Since A and B are mobile by definition, these points are moved on the fixed line: A-B, so that the slopes of the new lines at the points: $A + \Delta A$ and $B + \Delta B$, coincide with the field ratios: field according to z/field according to r, calculated at the previous points A and B. And so on, until the convergence of the alignment of the lines with the fields.

With this criterion, the alignment is obtained after 2 to 5 iterations. Let us take the example of a uniform field in space, then in this case, a single iteration is enough for the alignment of the slopes of the lines with the fields.

The assumed position of the Mx point is always defined as the intersection point of the lines C-A and D-B and can be determined in real time after 2 to 5 alignment convergence iterations. When the zero-field is reached at the Mx point, the lines C-A and D-B converge towards the separatrix and the fluxes at points A and B or C and D, are equal.

Thanks to this criterion, the lines always pass through the two fixed points C and D. The Mx point is a free zero-field point whose spatial position is defined only by the plasma current distribution and the amplitude of the JD currents.

This criterion makes it possible to determine the presumed position of the zero-field point in real time, when establishing the zero-field point (growth of JD currents). On the other hand, this method does not allow precise control of the presence and position of a zero-field point and it will be necessary to control, in real time, the fluxes at points C and D. Control of the fluxes at points A and B instead of C and D is also possible but under certain conditions of positioning of the line A-B, as explained in the following section.

9.5.5. Special condition of evaluating fluxes on the line AB

The fluxes generated at points A and B, by the only incoming current distribution: JD, of the divertor must satisfy the inequality, calculated with the mutual inductance in air:

$\Delta\emptyset = \emptyset_A(JD) - \emptyset_B(JD) < 0$, with points A and B positioned as in Figure 24.

It is practically the point with the greatest radial distance that sees the highest flux. On the contrary, with the only plasma current we obtain the opposite inequality, at the same points A and B. Indeed, when approaching the zero-field point, the lines AC and BD converge towards the separatrix where the fluxes at points A and B become equal. The zero-field point is reached when: $\Delta\emptyset = 0$.

It is necessary that the evolution of the mutual inductance of the divertor coil with the points of the line AB is a monotonically increasing function according to: r, in order to ensure the convergence of the slopes of the lines with the fields at points A and B and to evaluate the fluxes at these points.

In order to verify the previous property with the data of the Tokamak TORE SUPRA version WEST, we calculated the mutual inductance between the coil of the divertor and 40 points, increasing according to r, located on the line AB, parallel to the median plane of the coil and for three constant distances h according to the z axis of 15, 20 and 25 cm. The median

plane is defined, in the vertical plane: r, z, by the line passing through the centers of conductors 1 and 4 (4 conductors connected in series).

Figure 25 shows the three mutual inductance curves, calculated on the line AB parallel to the median plane of the coil, as a function of the distance h, along z, from the median plane of the coil. It can be seen that beyond point 31, for h=15 cm, the mutual inductance is no longer monotonically increasing along r. It is therefore necessary to modify the inclination of the line AB relative to the median plane of the divertor coil.

The correction consists of raising the height, along z, of point 1, from 20 cm to 35 cm and keeping the height of point 40 at 20 cm, values that allow segment AB to be kept inside the contour of the magnetic measurements. Figure 26 shows the evolution of the mutual with a straight-line AB whose left end (point 1) has been raised by 15 cm. This inclination correction ensures correct control of the fluxes at points A and B, whatever the positions of points A and B, with A always placed to the left of B.

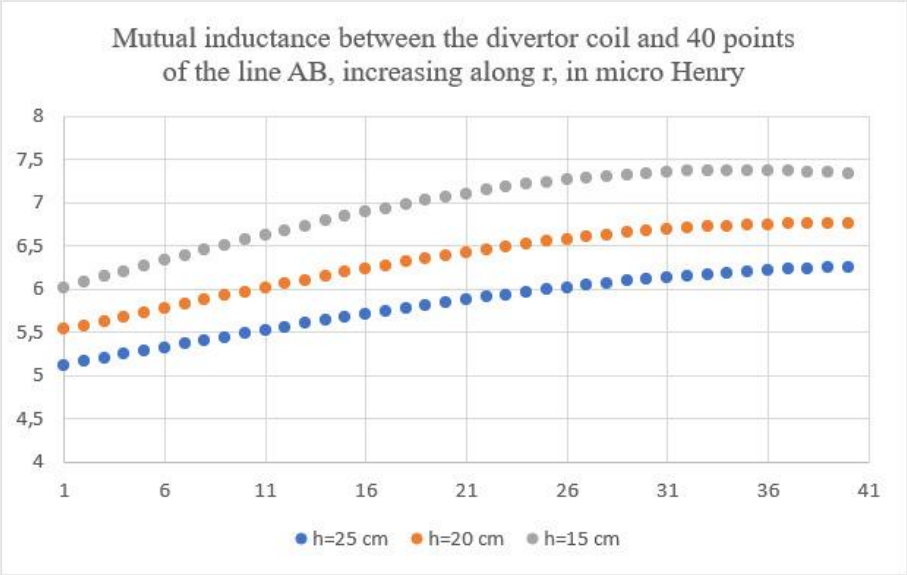

Figure 25

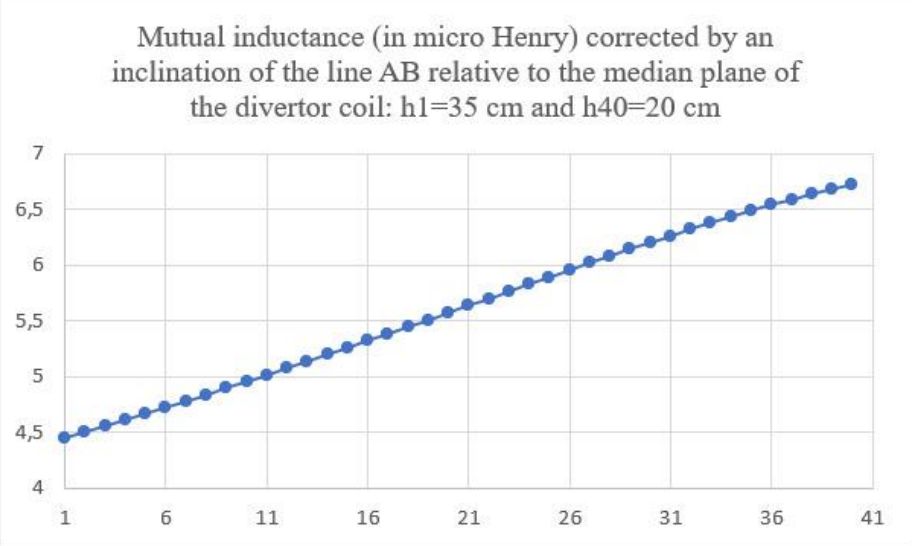

Figure 26

9.6. Application to the case of the WEST project of the TORE SUPRA machine

In the particular case of the WEST project, the plasma is coupled to a hybrid heating antenna which requires a plasma boundary passing exactly through 3 fixed points on the exterior side of the machine (UROG, EROG and LROG) in order to optimize the transfer of energy. (Figure 23). On the other hand, only one zero-field point is necessary at the bottom of the plasma with its control associated with the two points of the separatrix.

With regard to plasma position control, only the exact definition of the plasma boundary envelope matters, whether or not there are zero-field points. Plasma position control is therefore practically independent on the zero-field point control. On the other hand, it will be necessary to introduce the constraint of passing the plasma boundary through 3 fixed external points (UROG, EROG and LROG).

Plasma control will therefore be handled as follows:

a) Definition of the envelope Ce and a number of flux calculation points on the envelope: at least 40 points are necessary including the three external stress points. This is the most delicate work because it is necessary, for each point of the envelope, to calculate the angle of the tangent to Ce, at this point and to ensure that the envelope has a regular curvature.
b) Fixing an exact flux at the only external EROG point where the calculation of the plasma flux is carried out: $\Psi(1)$, for the calculation of the KBP matrix. The other two points will always be very close to the estimated values but there is, if necessary, the possibility of applying 2 additional constraints on the other two points in order to force the border to get closer to these points.
c) Control of plasma position according to § 9.3 with the reference point of the fluxes at point M(1) with: d(1)=0, at the EROG point. The calculation of the other distances d(i) is evaluated as prescribed in the relevant section. Then, the values of the flux deviations: $\Delta\Psi(i) = \Psi(i) - \Psi(1)$, on Ce of which calculated then reinjected into the loop. The KBP matrix will be calculated at least with the constraint of the exact flux at the EROG point N°1, using only the poloidal field coils.
d) The real-time poloidal coil voltages are the sum of a preprograming voltage (see § 9.2), a voltage generated by the plasma position loop and a voltage generated by the plasma current control loop.
e) The control of the zero-field point being independent from the plasma control, the method currently used can be re-applied but it is still possible to define a strategy without coupling physics by using a free zero-field point (see § 9.5).
f) Finally, the control of the plasma current can be done according to § 7.8.2.

Unfortunately, the collaboration with the TORE SUPRA team, in Cadarache, could not be initiated due to the lack of human resources and also the time allocated to carry out the modifications.

10. Main conclusion

10.1. Using only magnetic measurements associated with the poloidal field coils

This document shows, without detour, that the control of the plasma position and that of the amplitude of the plasma current can be carried out simply using only magnetic measurements for all Tokamak type machines with or without magnetic circuit and with or without magnetic "divertor". On the other hand, the processes implemented, thanks to these measurements, are simple, conventional, and based on the classical laws of electromagnetism. The plasma position loop being efficient (see below), the only poloidal field coils are sufficient for the control of the plasma position. It is shown that there exists a KBP matrix, of dimension NbxNp, which makes it possible to decouple the plasma position control loop from the vacuum chamber. Finally, there exists an optimal solution of the plasma position control loop (§ 7.5.4) with proportional matrix gain and scalar derivative gain, allowing high gains. With this solution, the convergence time constant is practically the same on all points of the reference contour and can be set between 10 ms and 100 ms.

Finally, the preprograming voltage required to compensate for the flux deviations generated by the currents of the magnetic divertors, if any, makes it possible to make the control of the zero-field points and the control of the plasma position, practically independent.

10.2. Magnetic measurements

In the "industrial" machines of the near future, magnetic measurements are essential elements for plasma control that require reliable, robust measurements with a high signal level in order to minimize electromagnetic pollution of the signal. As explained in § 6, only absolute flux measurements should be installed. Field measurements are useful but not essential for position and plasma current control. The plasma current is evaluated, with very good accuracy, by the sum of the ampere-turns of the internal distribution: Jp, which satisfies the flux measurements (§ 5).

The minimum number of absolute flux measurements, without redundancy, should be at least equal to: $N_{flux} = 12$, or about 17 to 20 measurements with redundancy in case of a faulty measurement.

10.3. Position control of a plasma with constrained boundary (fixed contour)

In the case of a machine without a magnetic divertor but with or without a magnetic circuit, the control of the plasma equilibrium would be achieved by reinjecting the flux differences: $\Delta\emptyset P$, calculated on Np (Np> Nb) points of the fixed contour of the plasma, at the level of the voltages of the poloidal field coils using the optimal solution developed in (§ 7.5.4).

10.4. Position control of a free boundary plasma (floating contour)

In the case of a “free” boundary plasma, for machines with or without a magnetic circuit, the evaluation of the flux deviations is carried out on the presumed boundary of the plasma calculated in real time and which is a moving contour located inside the envelope of the free boundaries of the plasma.

The flux deviations, thus calculated, are then reinjected at the level of the voltages of the poloidal field coils, as in the case of a fixed plasma contour but with a KBP matrix evaluated on the envelope of the plasma boundaries. The plasma position control loop remains the same as for a fixed plasma contour but the flux convergence time constants are this time slightly different.

In the case of machines with a magnetic divertor, the derivative of the currents of the divertor coils must be imperatively limited in maximum value so as not to destabilize the plasma (§ 9.2).

10.5. Zero-field point control for machines with divertor

We have suggested to control free zero-field points (§ 9.4.2), a process that does not require to calculate in real time the presumed position of the zero-field points and that does not distort the plasma boundary. This extremely simple process requires to control the flux difference between two fixed points, located on the coil of each divertor.

This only requires the installation of additional absolute flux loops, placed at the two fixed points of each divertor coil and an inductance connected in series with each divertor coil. Thus, the generator voltage associated with the divertor will be simply controlled with a simple proportional gain:

$$Vd = G * (\emptyset_C - \emptyset_D),$$ with G a positive real number.

Furthermore, as explained in § 9.2, it will be necessary to install the zero-field points by limiting the value of the derivative of the divertor currents so that the preprograming voltage generated to compensate for flux deviations at the envelope contour does not exceed 20% of the maximum value of each generator during the plasma current growth phase or the plasma current plateau phase. This limitation would be achieved, if necessary, using an external inductance connected in series with each divertor coil.

10.6. Voltage input of the poloidal field coils

The voltages of the poloidal field coils (or associated generators) are generally the sum of three signals:

- The voltage generated by the plasma position control loop,
- The voltage generated for controlling the amplitude of the plasma current (§ 7.8.2),
- The preprograming voltage for compensation of the plasma differential fluxes, generated by the growth of the “divertor” currents on the plasma envelope (§ 9.2).

10.7. Final conclusion

There is no simpler plasma control process than with only magnetic measurements associated with only poloidal field coils, mainly absolute fluxes. For a machine of the future, simplicity rhymes with reliability.

11. ANNEXE I: Basic documentation

11.1. Expression of complete elliptic integrals of the 1st and 2nd kind

The elliptic integrals of the first and second kind (LEGENDRE, Avril 1792) are involved in the expression of the magnetic field and this of the mutual inductances between coaxial circular wires. They are respectively defined by:

Equation 38: Elliptic integrals of first and second kind

$$K(k) = \int_0^{\frac{\pi}{2}} \frac{d\varphi}{\sqrt{1-k^2 sin^2\varphi}} \text{ and } E(k) = \int_0^{\frac{\pi}{2}} \sqrt{1-k^2 sin^2\varphi}\, d\varphi$$

They will be calculated using extremely convergent series (3 to 6 iterations depending on the precision: e = Abs(a-b), using the following algorithms:

Algorithme pour calculer $E(k, \epsilon_0)$

- $a \leftarrow 1$
- $b \leftarrow \sqrt{1-k^2}$
- $c \leftarrow k^2$
- $S \leftarrow c/2$
- $e \leftarrow S$
- Si $(k = 1)$: Retourner 1
- Sinon :
  - $n = 1$
  - Tant que $(e > \epsilon_0)$ faire :
    - $A \leftarrow (a+b)/2$
    - $B \leftarrow \sqrt{a \times b}$
    - $c \leftarrow A^2 - B^2$
    - $a \leftarrow A$
    - $b \leftarrow B$
    - $e \leftarrow 2^{n-1}c$
    - $S = S + e$
    - $n = n + 1$
  - Retourner $(1 - S) \times \pi/(2a)$

Figure 27: Algorithm for calculating E(k)

Algorithme pour calculer $K(k, \epsilon_0)$

- $a \leftarrow 1$
- $b \leftarrow \sqrt{1-k^2}$
- $e \leftarrow |a-b|$
- Tant que $(e > \epsilon_0)$ faire :
  - $c \leftarrow (a+b)/2$
  - $b \leftarrow \sqrt{a \times b}$
  - $a \leftarrow c$
  - $e \leftarrow |a-b|$
- Retourner $\pi/(2a)$

Figure 28: Algorithm for calculating K(k)

11.2. Expression of the magnetic field or induction created by a filiform circular wire at a point M in space

11.2.1. Documentation

According to the literature (MAXWELL, 1873), the calculation of the magnetic induction: $\vec{B}$, is obtained by integrating the vector potential: $\vec{A}$, on the circular wire then by calculating the magnetic induction according to the formula: $\vec{B} = rot\vec{A}$. The calculation of the magnetic field or induction requires the evaluation of the complete elliptic integrals of the first and second kind: $K(k)$ and $E(k)$.

The magnetic field: $\vec{H}$, is linked to the magnetic induction: $\vec{B}$, by: $\vec{B} = \mu_o \vec{H}$, in air or vacuum.

11.2.2. Formulation of the magnetic field at a point M in space

Consider a filiform circular wire (negligible conductor diameter) of large radius: a, located in a horizontal plane at altitude: Z= A, centered on the z axis and traversed by a current: I.

The magnetic field created by the wire at a point M (r, θ, z) in space is expressed in cylindrical coordinates according to the relations:

Equation 39: Expression of the magnetic induction created by a filiform circular wire at a point M in space and in air: $\mu_o = 4 * \pi * 10^{-7}$

$$k^2 = \frac{4 * a * r}{(r+a)^2 + (z-A)^2}$$

$$Br = \frac{\mu_o * I}{2\pi} * \frac{(z-A)}{r} * \frac{1}{[(r+a)^2 + (z-A)^2]^{0.5}} * \left[-K(k) + \frac{r^2 + a^2 + (z-A)^2}{(r-a)^2 + (z-A)^2} * E(k)\right]$$

$$B\theta = 0$$

$$Bz = \frac{\mu_o * I}{2\pi} * \frac{1}{[(r+a)^2 + (z-A)^2]^{0.5}} * \left[+K(k) + \frac{a^2 - r^2 - (z-A)^2}{(r-a)^2 + (z-A)^2} * E(k)\right]$$

11.3. Expression of the mutual inductance between two filiform coaxial circular wires

11.3.1. Documentation: Maxwell (GROVER F.W, 1916)

According to Maxwell (GROVER F.W, 1916), a famous mathematician of the 19th century, the mutual inductance between two filiform coaxial circular wires of large radii: a1 and a2, whose planes are distant along the axis Oz by the height: d12, is expressed according to the following basic formula with the elliptic integrals of the first and second kind as a function of k.

Equation 40: Basic expression of the mutual inductance between two coaxial circular wires

$$k = \frac{2 * (a1 * a2)^{0.5}}{[(a1 + a2)^2 + d12^2]^{0.5}}$$

$$M12 = \mu_o * (a1 * a2)^{0.5} * \left[\left(\frac{2}{k} - k\right) * K(k) - \frac{2}{k} * E(k)\right]$$

In the particular case where the two wires are very close, or even coincide, (case of the self-inductance of a wire), the value of k is: 1 and the function $K(k)$ diverges. Thus, the calculation of the inductance of a turn of circular wire (diameter: d) and large radius: a, will in this case be calculated by the Kirchhoff formula:

$$L = \mu_o * a * \left[Ln\left(16 * \frac{a}{d}\right) - \frac{7}{4}\right] \text{ with: } \frac{d}{a} < 0{,}05$$

Another simpler formulation of the mutual inductance evaluated by Maxwell and obtained by changing variables is presented below:

Equation 41: Other expression of the mutual inductance between two coaxial circular wires

$$M12 = 2 * \mu_o * \left(\frac{a1 * a2}{x}\right)^{0.5} * \left(K(x) - E(x)\right)$$

$$x = \frac{r1 - r2}{r1 + r2}$$

$$r1 = ((a1 + a2)^2 + d12^2)^{0.5} \ and \ r2 = ((a1 - a2)^2 + d12^2)^{0.5}$$

This time, the elliptic integrals are evaluated from the parameter: x different of k.

11.4. Expression of mutual inductances between machine conductors

The different conductors of the machine including the poloidal field coils, the « divertor » coils and the vacuum chamber are modelled by a set of coaxial circular conductors arranged according to a geometry specific to the contour. The mutual inductances between the different conductors are therefore generated by averages calculations between contours from the fluxes created by coaxial circular wires.

12. ANNEXE II: Implementation of numerical calculations

The basic functions and subprograms defined below were created with VBA (Visual Basic for Application) language, included in Microsoft Excel and therefore accessible to everyone. All programming, defined below, can be easily transposed into other programming languages like Fortran, Python, MATLAB, etc.

12.1. Calculation and verification of elliptic integrals of the 1st and 2nd kind

The elliptic integrals $K(k)$ and $E(k)$ are evaluated by functions calculating rapidly convergent sequences with a precision criterion, according to the algorithms in § 11.1.

```
Function IntElipK(k As Double, precision As Double) As Double
    Dim a As Double, b As Double, e As Double, C As Double, pi As Double
    a = 1
    b = (1 - k * k) ^ 0.5
    e = Abs(a - b)
100 If e < precision Then GoTo 50 Else
    C = (a + b) / 2
    b = (a * b) ^ 0.5
    a = C
    e = Abs(a - b)
    GoTo 100

50  pi = Application.WorksheetFunction.pi
    IntElipK = pi / (2 * a)
End Function
```

Figure 29: Function calculating K(k)

```
Function IntElipE(k As Double, precision As Double) As Double
    Dim a As Double, b As Double, e As Double, C As Double, pi As Double
    Dim S As Double, Ga As Double, Gb As Double
    Dim N As Long

    If k = 1 Then GoTo 60
    a = 1
    b = (1 - k * k) ^ 0.5
    C = k * k
    S = C / 2
    e = S
    N = 1

100 If e < precision Then GoTo 50 Else
    Ga = (a + b) / 2
    Gb = (a * b) ^ 0.5
    C = Ga * Ga - Gb * Gb
    a = Ga
    b = Gb
    e = C * 2^ ^ (N - 1)
    S = S + e
    N = N + 1
    GoTo 100

50  pi = Application.WorksheetFunction.pi
    IntElipE = (1 - S) * pi / (2 * a)
    GoTo 70

60  IntElipE = 1
70
End Function
```

Figure 30: Function calculating E(k)

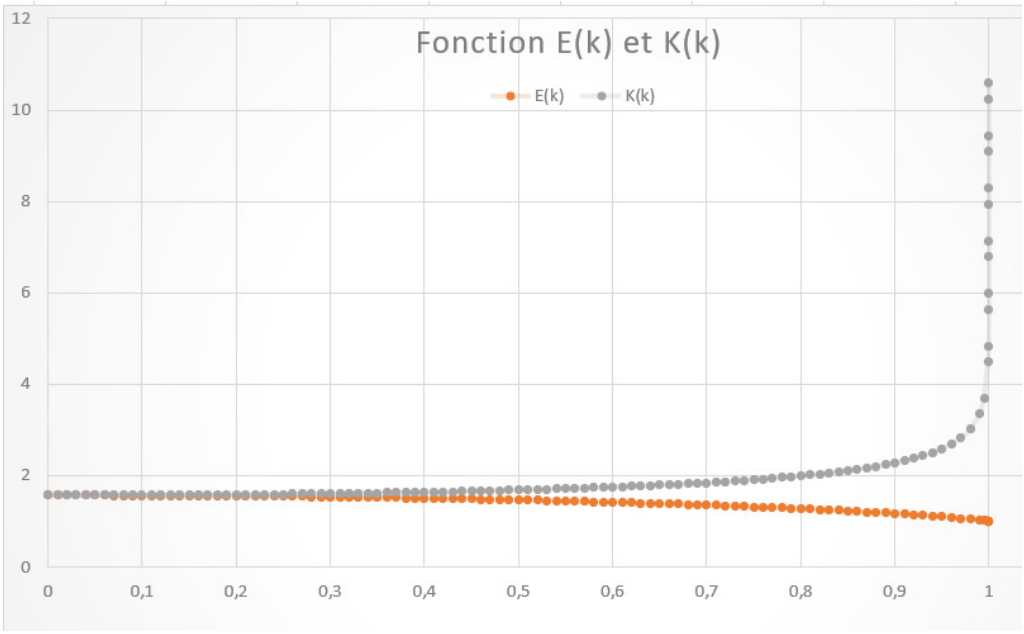

Figure 31: Evolution of the elliptic integrals E(k) and K(k) versus k

In general, a precision of 10^{-3} is sufficient with the exception of the calculation of $K(k)$ in the vicinity of k=1 where a precision of 10^{-6} or 10^{-7} is required in certain cases: very close wires or calculation of the magnetic field in the vicinity of the conductor.

12.2. Calculation of the magnetic field created by a filiform circular wire

The calculation of the magnetic field (induction) is carried out according to the formulation of § 11.2.2 in Equation 39.

This calculation is carried out in the subroutine below. As it is not impossible, with VBA to directly express the Br and Bz values, components of the magnetic induction as an external argument, of the main program; the latter has been transformed into two independent functions BR and BZ which calculate these values individually.

The arguments are:

- Point M defined by: M(r, z).
- Circular wire defined by: Ra=large radius and Za=altitude according to Oz of the plane of the wire.
- Precision = parameter for calculating elliptic integrals (10^{-3} to 10^{-6}).

```
Function BR(r As Double, z As Double, Ra As Double, Za As Double, precision As Double) As Double
' r et z: coordonnées du point M
'Ra et Za: grand rayon Ra et altitude du plan de la spire Za
'
Dim h As Double, B As Double, C As Double, D As Double, e As Double
Dim k As Double, FK As Double, FE As Double
Dim Eps As Double
'
Eps = 0.0000002
'
h = z - Za
B = ((Ra + r) * (Ra + r) + h * h)
C = ((Ra - r) * (Ra - r) + h * h)
D = (Ra * Ra - r * r - h * h)
e = (Ra * Ra + r * r + h * h)
'
k = (4 * Ra * r / B) ^ 0.5
'
FE = IntElipE(k, precision)
FK = IntElipK(k, precision)
'
'Bz = Eps * (B ^ -0.5) * (FK + (D / C) * FE)
BR = Eps * (h / r) * (B ^ -0.5) * (-FK + (e / C) * FE)
'
'MsgBox "Br=" & BR & "   Bz=" & BZ & "     k=" & k
End Function
```

Figure 32: Function evaluating the radial field Br

```
Function BZ(r As Double, z As Double, Ra As Double, Za As Double, precision As Double) As Double
' r et z: coordonnées du point M
'Ra et Za: grand rayon Ra et altitude du plan de la spire Za
'
Dim h As Double, B As Double, C As Double, D As Double, e As Double
Dim k As Double, FK As Double, FE As Double
Dim Eps As Double
'
Eps = 0.0000002
'
h = z - Za
B = ((Ra + r) * (Ra + r) + h * h)
C = ((Ra - r) * (Ra - r) + h * h)
D = (Ra * Ra - r * r - h * h)
e = (Ra * Ra + r * r + h * h)
'
k = (4 * Ra * r / B) ^ 0.5
'
FE = IntElipE(k, precision)
FK = IntElipK(k, precision)
'
BZ = Eps * (B ^ -0.5) * (FK + (D / C) * FE)
'BR = Eps * (h / r) * (B ^ -0.5) * (-FK + (E / C) * FE)
'
'MsgBox "Br=" & BR & "   Bz=" & BZ & "     k=" & k
End Function
```

Figure 33: Function evaluating the vertical field Bz

The BR and BZ functions were tested by calculating the circulation of the magnetic field on a circular contour of radius: e, and centered on the conductor (Ra) with e < Ra. The circulation of $H=B/\mu_o$ on the previous circular contour returns the value: 1 and the value 0 in the case where the contour does not encircle the conductor. Below is the control subroutine:

```
'Calcul de la circulation du champ sur un contour circulaire centré sur le conducteur

Sub CirculationChamp()
Dim Ra As Double, Za As Double, x As Double, r As Double, z As Double, e As Double
Dim Hr As Double, Hz As Double
Dim precision As Double, pi As Double, V As Double
Dim N As Integer, I As Integer
'
precision = 0.000001
pi = 3.14159265358979
N = 1000
Ra = 2
Za = 0
e = 1
'
V = 0
For I = 1 To N
x = 2 * pi * (I - 1) / N
r = Ra + e * Cos(x)
z = e * Sin(x)
'
Hr = 10000000 * BR(r, z, Ra, Za, precision) / 4 / pi
Hz = 10000000 * BZ(r, z, Ra, Za, precision) / 4 / pi
'
V = V + (Hr * Sin(x) - Hz * Cos(x)) * e * 2 * pi / N
'
Next

MsgBox "V=" & V

End Sub
```

Figure 34: Subroutine evaluating the field circulation on a closed contour

12.3. Calculation of mutual inductances between coaxial circular wires

The calculation of the mutual inductances between two distant coaxial circular wires can be carried out using one of the two formulas established by Maxwell, shown in § 11.3. We selected the expression of Equation 40, more classic than Equation 41 and easier to investigate the value of K(k) in the vicinity of k=1. Both expressions have been tested and of course give the same numerical result. Below is the function: MUT12, expressed according to Equation 40.

```
'Première formulation de Maxwell:
'
Function MUT12(a1 As Double, a2 As Double, d12 As Double, e As Double, precision As Double)
'a1=rayon spire 1
'a2=rayon spire 2
'd12=distance entre les plans des spires
'e=petit diametre ou épaisseur du conducteur des spires
'
Dim k As Double
Dim FE As Double, FK As Double
Dim pi As Double, Eps As Double
'
pi = 3.14159265358979
Eps = 0.0000001
'
k = (4 * a1 * a2 / ((a1 + a2) * (a1 + a2) + d12 * d12)) ^ 0.5
'
If d12 = 0 And a1 = a2 Then GoTo 100 Else
FK = IntElipK(k, precision)
FE = IntElipE(k, precision)
MUT12 = 4 * pi * Eps * ((a1 * a2) ^ 0.5) * ((2 / k - k) * FK - 2 * FE / k)
Exit Function
100
'inductance pure selon Kirchhoff
MUT12 = 4 * pi * Eps * a1 * (Log(16 * a1 / e) - 7 / 4)
End Function
```

Figure 35: Function calculating the mutual inductance between coaxial circular wires

12.4. Calculation of mutual inductances of the poloidal field coils

The spatial data of the coil configuration are presented in an Excel table with the data (R, Z) of the planes delimiting the section of the coils in a coordinate system passing through the Oz axis of the machine (these data do not correspond to any existing machines. They were chosen arbitrarily for the example).

N°Bobine	R1 (m)	R2 (m)	Z1(m)	Z2(m)
1	1,00	1,30	-0,60	0,60
2	1,50	1,75	0,80	1,05
3	2,00	2,30	1,30	1,60
4	2,75	3,00	0,80	1,00
5	3,00	3,30	-0,40	0,40
6	2,75	3,00	-1,00	-0,80
7	2,00	2,30	-1,60	-1,30
8	1,50	1,75	-1,05	-0,80

Table 4: Definition of the poloidal field coils

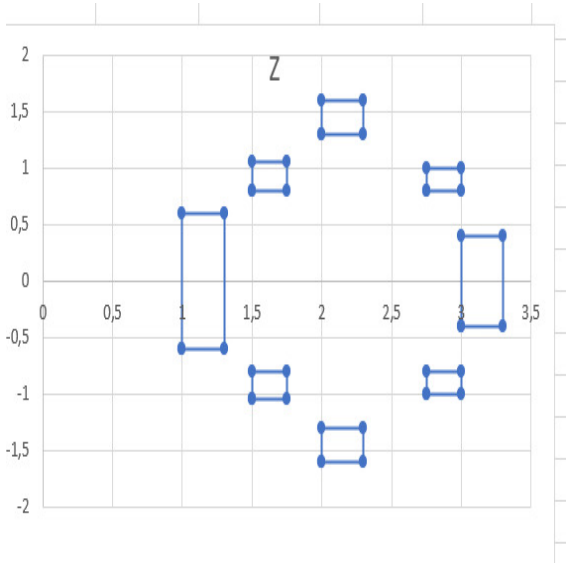

Figure 36: Vertical section showing the arrangement of the coils described in the previous table

The rectangular cross section of each coil is modelled by: Nr*Nz, turns of circular section whose conductor diameter is equal to: Emin.

If Nt is the desired maximum number of turns included in the section then Nt >= Nr*Nz:

$$Emin(i) = \sqrt{\frac{|R2(i) - R1(i)| * |Z2(i) - Z1(i)|}{Nt}} \quad for\ i = 1\ to\ Nb$$

We deduce:

$$NR(i) = Entire\ part\ of : \frac{|R2(i)-R1(i)|}{Emin(i)}\ and\ NZ(i) = Entire\ part\ of : \frac{|Z2(i)-Z1(i)|}{Emin(i)}$$

Assuming that the conductors located on the perimeter of the section are tangent to it, then the conductors are spaced by a distance DR along R and DZ along Z calculated by:

$$DR(i) = \frac{|R2(i) - R1(i)| - NR(i) * Emin(i)}{NR(i) - 1}\ and\ DZ(i) = \frac{|Z2(i) - Z1(i)| - NZ(i) * Emin(i)}{NZ(i) - 1}$$

Then, with: R1(i) < R2(i) and Z1(i) < Z2(i),), the parameters of the mutual inductance between the two wires are the two large radii: a1 and a2, and the distance between the planes of the wires d12:

$$a2 = R1(j) + \frac{Emin(j)}{2} + \big(Emin(j) + DR(j)\big) * (Kr(j) - 1)\ and\ Kr(j) = 1\ to\ NR(j)$$

$$d12 = \left[Z1(j) + \frac{Emin(j)}{2} + \big(Emin(j) + DZ(j)\big) * (Kz(j) - 1)\right] - \left[Z1(i) + \frac{Emin(i)}{2} + \big(Emin(i) + DZ(i)\big) * (Kz(i) - 1)\right]$$

$$and\ Kz(i) = 1\ to\ NZ(i)\ and\ Kz(j) = 1\ to\ NZ(j)$$

The full subroutine for the mutual inductance calculation is not displayed because of the excessive size. For simplifying the calculation and comparing the results, the total number of elementary conductors in each coil section is the same: Nt.

The following table shows the results of mutual inductance calculations with an accuracy of 10^{-6} and for different values of Nt from 100 to 500. There are no notable differences. Only self-inductances are assigned to the 3rd decimal place.

100	**2,012262191625E-06**	1,038236548219E-06	6,759355407334E-07	8,095687752869E-07	8,540133164087E-07	8,095687752869E-07	6,759355407334E-07	1,038236548219E-06
		5,641331953590E-06	2,543253993437E-06	2,091853952144E-06	1,538541735703E-06	1,033985837038E-06	6,103905622328E-07	6,612763164933E-07
			7,725660963532E-06	3,608891119911E-06	2,137763320196E-06	1,249353339362E-06	6,596990548746E-07	6,103905622328E-07
				1,240856733173E-05	4,983458260335E-06	2,554412751863E-06	1,249353339362E-06	1,033985837038E-06
					1,043843665132E-05	4,983458260334E-06	2,137763320196E-06	1,538541735703E-06
						1,240856733173E-05	3,608891119911E-06	2,091853952144E-06
							7,725660963532E-06	2,543253993437E-06
								5,641331953590E-06
200	**2,010616816374E-06**	1,038395826361E-06	6,760284767698E-07	8,096710991188E-07	8,541203520276E-07	8,096710991188E-07	6,760284767698E-07	1,038395826361E-06
		5,638373100364E-06	2,543279989186E-06	2,091875995043E-06	1,538562484231E-06	1,033999905700E-06	6,104000521932E-07	6,612871341955E-07
			7,721734982452E-06	3,608931253483E-06	2,137783197709E-06	1,249366748544E-06	6,597085226664E-07	6,104000521932E-07
				1,241236720357E-05	4,983491222821E-06	2,554428343815E-06	1,249366748544E-06	1,033999905700E-06
					1,044645384739E-05	4,983491222821E-06	2,137783197710E-06	1,538562484231E-06
						1,241236720357E-05	3,608931253483E-06	2,091875995043E-06
							7,721734982452E-06	2,543279989186E-06
								5,638373100364E-06
300	**2,012517328657E-06**	1,038325141230E-06	6,759991866845E-07	8,096509931350E-07	8,541038814732E-07	8,096509931350E-07	6,759991866845E-07	1,038325141230E-06
		5,637117855506E-06	2,543289858143E-06	2,091876176522E-06	1,538566902232E-06	1,034006186300E-06	6,104036032376E-07	6,612911809719E-07
			7,720070125373E-06	3,608939285974E-06	2,137791744673E-06	1,249374384718E-06	6,597120653895E-07	6,104036032376E-07
				1,240136376279E-05	4,983532511817E-06	2,554448629220E-06	1,249374384718E-06	1,034006186300E-06
					1,044392604403E-05	4,983532511817E-06	2,137791744673E-06	1,538566902232E-06
						1,240136376279E-05	3,608939285974E-06	2,091876176522E-06
							7,720070125373E-06	2,543289858143E-06
								5,637117855506E-06

Figure 37: Coils mutual inductance for Nt=100, 200 and 300

400	**2,010888666472E-06**	1,038399761988E-06	6,760441343433E-07	8,097081874625E-07	8,541799815106E-07	8,097081874625E-07	6,760441343433E-07	1,038399761988E-06
		5,639021359196E-06	2,543282915255E-06	2,091879112059E-06	1,538571871828E-06	1,034001646953E-06	6,104016297655E-07	6,612889434381E-07
			7,722591062463E-06	3,608933560668E-06	2,137749358149E-06	1,249369063704E-06	6,597100967873E-07	6,104016297655E-07
				1,240526740455E-05	4,983215424808E-06	2,554432348826E-06	1,249369063704E-06	1,034001646953E-06
					1,043996686776E-05	4,983215424808E-06	2,137749358149E-06	1,538571871828E-06
						1,240526740455E-05	3,608933560669E-06	2,091879112059E-06
							7,722591062463E-06	2,543282915255E-06
								5,639021359196E-06
500	**2,010528946630E-06**	1,038400986124E-06	6,760539560647E-07	8,097346971642E-07	8,542084393289E-07	8,097346971642E-07	6,760539560647E-07	1,038400986124E-06
		5,637404657879E-06	2,543291662145E-06	2,091882659805E-06	1,538575861677E-06	1,034006751694E-06	6,104045245209E-07	6,612922368030E-07
			7,720448264132E-06	3,608945395888E-06	2,137767136359E-06	1,249374246843E-06	6,597129846410E-07	6,104045245209E-07
				1,240588818556E-05	4,983321846269E-06	2,554442561769E-06	1,249374246843E-06	1,034006751694E-06
					1,044325896298E-05	4,983321846268E-06	2,137767136359E-06	1,538575861677E-06
						1,240588818556E-05	3,608945395888E-06	2,091882659805E-06
							7,720448264132E-06	2,543291662145E-06
								5,637404657879E-06

Figure 38: Coils mutual inductance for Nt=400 and 500

The necessary value of: precision, depends on the value of 1-k, in the vicinity of k=1. In the case of poloidal field coils, the minimum value of 1-k is the value obtained for two wires of the same radius a but separated by d12=Emin, i.e. in this case:

$$1 - k = \frac{Emin^2}{8 * a^2}$$

During the previous calculations this value of: 1-k, remains greater than 10^{-7} for Nt max =500 and the calculation of K(k) requires in this case a precision of: 10^{-4}.

We must also not forget that the value of the inductance of a circular wire (§ 11.3.1) is a correct approximate value for: Emin /a < 0.05, which means that it is necessary to select a minimum number of turns: Nt, in the section of the coils to satisfy this criterion, or in our case, greater than Nt >= 200 for the central coil N°1.

References

1. GROVER F.W, R. E. (1916). Formulas and Tables for Calculation of Mutual Inductances (Revised).
2. LAGRANGE, J. L. (1788). Mécanique analytique (Multiplicateur de Lagrange).
3. LEGENDRE, A.-M. (Avril 1792). Mémoire sur les transcendantes elliptiques. Paris.
4. MAXWELL, J. C. (1873). Treatise on Electricity and Magnetism (Vol.1 and Vol.2). Oxford.

Copyright: ©2025 Bernard Bareyt. This is an open-access article distributed under the terms of the Creative Commons Attribution License, which permits unrestricted use, distribution, and reproduction in any medium, provided the original author and source are credited.